





# Primordial Black Holes from Inflation with a Spectator Field

Dario L. Lorenzoni <sup>1,2,\*</sup> Sarah R. Geller <sup>3,4,5,†</sup> David I. Kaiser <sup>6,‡</sup> and Evan McDonough <sup>2,§</sup>

<sup>1</sup>*Department of Physics & Astronomy, University of Manitoba, Winnipeg, MB R3T 2N2, Canada*

<sup>2</sup>*Department of Physics, University of Winnipeg, Winnipeg, MB R3B 2E9, Canada*

<sup>3</sup>*Santa Cruz Institute for Particle Physics, Santa Cruz, CA 95064, USA*

<sup>4</sup>*Department of Physics, University of California, Santa Cruz, Santa Cruz, CA 95064, USA*

<sup>5</sup>*Department of Astronomy, Yale University, Kline Tower,  
266 Whitney Avenue, New Haven, CT 06511, USA*

<sup>6</sup>*Department of Physics, Massachusetts Institute of Technology, Cambridge, MA 02139, USA*

How is the production of primordial black holes (PBHs) in single-field models of inflation impacted by the presence of additional scalar fields? We consider the effect of a spectator field—a free scalar field with sub-Hubble mass, no direct coupling to the inflaton, and which makes a subdominant contribution to the total energy density—in the context of single-field models of inflation featuring a transient phase of ultra-slow roll (USR) evolution. Despite the modest title, a spectator field can have a dramatic impact: the slow-roll evolution of the spectator prevents the combined inflaton-and-spectator system from entering into USR, which naively might be expected to preclude the production of PBHs. However, we demonstrate that the growth of perturbations is maintained or enhanced by the spectator, through the rich interplay of curvature and isocurvature perturbations. We show in a model-independent way that the single-field phase of ultra-slow-roll is replaced by two turns in field space encompassing a phase of tachyonic instability for the isocurvature perturbations and a transfer of power from isocurvature to curvature modes. Furthermore, we highlight a degeneracy between the fine-tuning of the feature in the inflaton potential and the parameters of the spectator, leading to an overall *resilience* of model predictions to parameter variations. This makes it easier for the underlying PBH model to accommodate both high-precision CMB constraints and production of PBHs in the asteroid-mass range.

## I. INTRODUCTION

Primordial black holes (PBHs) [1–7] have a long and storied history, predating the modern era of precision cosmology. In recent years, PBHs have emerged as a leading candidate to explain some or all of the observed dark matter [8–17]. Primordial black holes may also explain the JWST observations of high-redshift supermassive black holes [18–22], and a variety of observations, from gravitational waves at LIGO [23], NANOGrav [24, 25], and future detectors [26], to ultrahigh-energy neutrinos [27, 28] and other cosmic rays [29]. In all these cases the question that remains is the origin of the large density fluctuations necessary for the direct collapse formation of PBHs.

The origin of PBHs finds a natural home in models of cosmic inflation.<sup>1</sup> Inflation provides a causal mechanism for structure formation, with primordial perturbations observed in the cosmic microwave background (CMB) and large-scale structure originating from quantum fluctuations. It is possible these same quantum fluctuations, on much shorter length scales than those directly probed

by the CMB, could seed the formation of primordial black holes.

A significant body of work has been dedicated to this possibility. For example, single-field inflation models with a potential  $V(\varphi)$  that is tuned to yield a brief period of ultra-slow-roll (USR) evolution can lead to an enhancement of perturbations on a characteristic scale, resulting in a spike in the primordial power spectrum of curvature perturbations [36–60]. However, the demand that the model both satisfy CMB constraints [61–64] and produce a population of PBHs consistent with observations [8–17], places a significant restriction on model building. In the context of single-field USR models, this manifests as a significant parameter fine-tuning [52], in the sense that the predictions of the model are exponentially sensitive to small variations in one or more model parameters.

On the other hand, it is not *a priori* the case that the early universe can be described by a single scalar field. The realm of particle physics is far from single-field: the Higgs doublet of the Standard Model comprises four real scalars, and particle physics theories beyond the Standard Model (such as the two-Higgs-doublet model [65]) typically add yet more scalars [66, 67]. String theory provides another example, with potentially many moduli fields at low energies, including the string theory axiverse, which could add up to *tens of thousands* of axion-like particles to the spectrum [68]. Field theory models can also yield an axiverse-like spectrum [69–72]. It stands to reason that the dynamics of cosmic inflation could rely on multiple scalar fields, usually termed “multifield inflation.”

Multifield inflation offers ample opportunities for PBH

\* [lorenzod@myumanitoba.ca](mailto:lorenzod@myumanitoba.ca)

† [sageller@ucsc.edu](mailto:sageller@ucsc.edu)

‡ [dikaizer@mit.edu](mailto:dikaizer@mit.edu)

§ [e.mcdonough@uwinnipeg.ca](mailto:e.mcdonough@uwinnipeg.ca)

<sup>1</sup> Alternative production mechanisms include bubble collision [30, 31], collapse of cosmic strings [32, 33] or domain walls [34], quark confinement [35], and others. These mechanisms are beyond the scope of our work; for a review of these processes, see Refs. [8, 16].

production [26, 73–86]. Such models typically consider a direct coupling between the different fields, either in the kinetic sector or in their potential or both, and may include multiple distinct phases of inflation driven by the different scalar fields of the model.

A minimal realization of multifield inflation is given by the seemingly trivial case of a *spectator field*, which is subdominant in energy density to the inflaton and, in its minimal realization, has no direct coupling to the inflaton. The spectator ostensibly plays no role in the background evolution, but can have important phenomenological implications: Spectator fields can source CMB non-Gaussianity [87], gravitational waves [88–90], and jointly the matter-antimatter asymmetry and production of dark matter [91], among other signatures.

In this work, and in the accompanying letter [92], we consider the influence of spectator fields in the context of single-field models of PBH production. The spectator field is defined as a free scalar field with no direct coupling to the inflaton, with a mass that is small compared to Hubble scale during inflation, and which makes a subdominant contribution to the energy density at all times. In this companion paper we expand upon the origin and phenomenological implications of the spectator scenario presented in Ref. [92], in which one of many available single-field USR PBH models is supplemented with a simple spectator field.

Our main finding is that the inclusion of a spectator field as defined above can maintain or enhance the production of primordial black holes in single-field models, despite significantly altering the dynamics of both the background evolution and perturbations. Notably, *the spectator can prevent the system from ever entering a phase of ultra-slow-roll, and yet still realize the enhancement of perturbations required to seed PBHs*. The would-be USR enhancement is supplanted by a tachyonic growth of isocurvature perturbations, which is converted to curvature perturbations during a turn in field space.

With the requirement of USR removed, so too is the extreme fine-tuning of the feature in the potential. The spectator therefore imbues the single-field PBH model with a *resilience* to small variations in the inflaton model parameters. While the feature in the potential is still a required ingredient, the degree of precision with which the single-field model parameters must be specified is significantly reduced. As we detail in this companion paper and the accompanying letter [92], this is realized through a compensation between inflaton model parameters and  $\mathcal{O}(1)$  variations in the spectator parameters. This indicates that this setup may alleviate the well-known issue of fine-tuning in single-field models of inflation that produce PBHs, by considering the physically motivated presence of additional fields.

This manuscript is structured as a comparison between our Spectator PBH scenario and the single-field models upon which it is built. We begin by introducing the background dynamics of both setups in Section II, in which we review the physics of ultra-slow-roll inflation before

delving into the multifield dynamics. Section III describes the formation of inflationary perturbations and highlights the differences and similarities between the single-field and Spectator PBH scenarios. The shape of the curvature power spectrum is analyzed in Section IV, in which we explicitly show consistency with CMB constraints and with the production of PBHs in the so-called asteroid-mass range, with  $10^{17} \text{ g} \leq M_{\text{PBH}} \leq 10^{23} \text{ g}$ . The dependence of the model (and its observables) on both the inflaton and spectator parameters is the subject of Section V. While we consider, for simplicity, a particular form of the inflaton potential throughout the previous sections, we show in Section VI that this mechanism is generic to single-field inflation models that produce PBHs through a phase of USR evolution. Finally, we summarize and discuss our results in VII, in which we highlight future research directions.

## II. THE SPECTATOR PBH MODEL: BACKGROUND EVOLUTION

Single-field models of inflation can produce PBHs through a transient phase of ultra-slow-roll (USR), during which the evolution of the inflaton field,  $\varphi$ , slows down. As we will see in Section III, this amplifies curvature perturbations, enhancing the inflationary power spectrum on appropriate scales and allowing for the formation of PBHs.

We begin by asking a simple question: *what would happen to PBH production in these single-field models of inflation if another scalar field were to simply exist in the Universe?* Such a field would be *spectating* inflation, having no direct coupling to the inflaton and a subdominant contribution to the energy density of the Universe. Including the presence of this spectator field,  $\chi$ , the action of the system becomes

$$S = \int d^4x \sqrt{-g} \left[ \frac{M_{\text{Pl}}^2}{2} R - \frac{1}{2} (\partial\varphi)^2 - \frac{1}{2} (\partial\chi)^2 - V(\varphi, \chi) \right], \quad (1)$$

where  $M_{\text{Pl}} \equiv 1/\sqrt{8\pi G}$  is the reduced Planck mass, and  $g$  and  $R$  are the determinant of the spacetime metric and its Ricci scalar. The potential of the system is simply given by the sum of the inflaton and spectator contributions:

$$V(\varphi, \chi) = V_{\text{PBH}}(\varphi) + V_S(\chi), \quad (2)$$

with the inflaton potential being of the PBH-producing kind, supporting a phase of USR.

There are therefore *no direct couplings* between the inflaton and the spectator field in this setup, neither in the kinetic sector nor in the potential. The mechanism on which we focus here requires neither a curved field-space manifold with its associated noncanonical kinetic sector nor multiple phases of inflation. This setup is thus starkly different from the ones considered in the literature, which explicitly depend on some kind of field coupling [26, 73–84, 86].

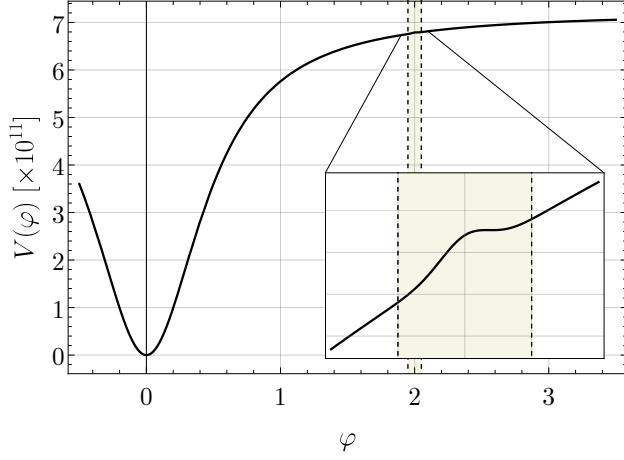


FIG. 1. The inflationary potential  $V_{\text{PBH},A}$  of Eq. (4), in units of  $M_{\text{Pl}}$ . The inset highlights the presence of a local inflection point that causes the inflaton field to slow down as it rolls down the potential, yielding a temporary phase of ultra-slow-roll (USR) evolution. The parameters used in this figure are delineated in the “Reference” row of Table I.

### A. Single-Field Inflation

Let us first review the dynamics of PBH-producing single-field models in the absence of spectator fields, i.e. setting  $V_S(\chi) = 0$  and  $\chi = 0$  in Eq. (1):

$$S = \int d^4x \sqrt{-g} \left[ \frac{M_{\text{Pl}}^2}{2} R - \frac{1}{2} (\partial\varphi)^2 - V_{\text{PBH}}(\varphi) \right]. \quad (3)$$

In order to support a phase of ultra-slow-roll evolution, the inflaton potential  $V_{\text{PBH}}(\varphi)$  needs to exhibit a local feature that will cause the field to temporarily slow down its evolution. This requires the potential to be nearly flat, such as in the vicinity of a (quasi-)inflection point. As a concrete example, consider the potential of Ref. [48],

$$V_{\text{PBH},A}(\varphi) = V_0 \frac{\varphi^2}{\varphi^2 + M^2} \left( 1 + A e^{-(\varphi - \varphi_d)^2 / 2\sigma^2} \right), \quad (4)$$

which superimposes a Gaussian “bump” (of width  $\sigma$ , at position  $\varphi_d$ ) on the well-known KKLT potential [93]. The shape of  $V_{\text{PBH},A}$  is illustrated in Fig. 1, for the reference model parameters of Table I: a local minimum appears, followed by a local maximum. (This feature could also be a plateau region.) We will adopt this potential in the following discussion, and will show in Section VI that the mechanism described hereafter is independent of the particular form of  $V_{\text{PBH}}$ .

The background evolution of the inflaton field is governed by its equation of motion and by the Friedmann equation,

$$\ddot{\varphi} + 3H\dot{\varphi} = -\partial_\varphi V_{\text{PBH}}, \quad (5)$$

$$H^2 = \frac{1}{3M_{\text{Pl}}^2} \left( \frac{\dot{\varphi}^2}{2} + V_{\text{PBH}} \right). \quad (6)$$

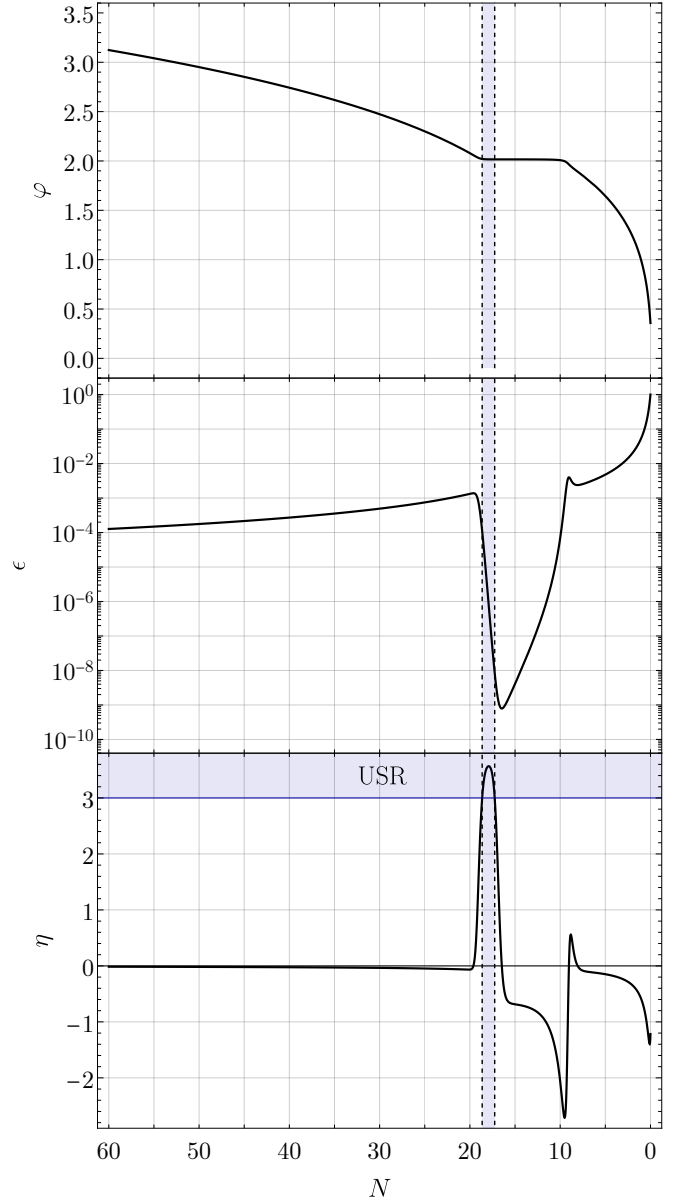


FIG. 2. Evolution of the background field  $\varphi$  and of the slow-roll parameters  $\epsilon$  and  $\eta$  in the single-field regime of Eq. (3). This is shown for the  $V_{\text{PBH},A}$  potential of Eq. (4), using the “Reference” model parameters of Table I. The time evolution is shown in terms of the number of e-folds  $N$  before the end of inflation, see Eq. (12). *Top panel:* The inflaton  $\varphi$  rolls slowly down its potential at the beginning and at the end of its evolution. When it reaches the feature in  $V_{\text{PBH},A}$ ,  $\varphi$ ’s evolution is considerably slowed down ( $\varphi$  barely evolves during  $20 \lesssim N \lesssim 10$ ) until it evolves beyond the feature. *Middle panel:* As the inflaton is slowed down by the feature in  $V_{\text{PBH},A}$ , the slow-roll parameter  $\epsilon$  quickly decreases from  $\mathcal{O}(10^{-4})$  to  $\mathcal{O}(10^{-9})$ . It increases again as  $\varphi$  picks up speed after the local feature, eventually reaching the value  $\epsilon = 1$  and ending the inflationary epoch. *Bottom panel:* The significant slowing down of the field causes a temporary phase of ultra-slow-roll: as  $\epsilon$  decreases,  $\eta$  becomes large, crossing into the USR regime for 1.4 e-folds. *All panels:* The shaded region highlights the phase of ultra-slow-roll  $\eta \geq 3$ .

The dot notation indicates time derivatives, while  $\partial_\varphi = \partial/\partial\varphi$  denotes differentiation with respect to the field  $\varphi$ . The Friedmann equation (6) relates the field dynamics to the expansion of space, encoded in the Hubble parameter  $H = \dot{a}/a$ , where  $a$  is the scale factor of the Universe. The inflationary dynamics can be described by the slow-roll parameters

$$\epsilon \equiv -\frac{\dot{H}}{H^2} = \frac{1}{2} \frac{\dot{\varphi}^2}{H^2 M_{\text{Pl}}^2}, \quad (7)$$

$$\eta \equiv 2\epsilon - \frac{\dot{\epsilon}}{2H\epsilon}. \quad (8)$$

Inflation (namely, accelerated expansion of space) requires  $\epsilon < 1$ , while *slow-roll* inflation refers to the regime  $\epsilon \ll 1$  and  $|\eta| \ll 1$ . *Ultra* slow-roll (USR) inflation occurs when  $\epsilon \ll 1$  but  $\eta \geq 3$ , corresponding to the condition that  $\partial_\varphi V_{\text{PBH}}$  is a subdominant contribution to the field's equation of motion, Eq. (5). In summary,

$$\text{SR: } \epsilon \ll 1, \quad |\eta| \ll 1, \quad (9)$$

$$\text{USR: } \epsilon \rightarrow 0^+, \quad \eta \geq 3. \quad (10)$$

In the vicinity of a (quasi-)inflection point, the potential flattens and its derivative  $\partial_\varphi V_{\text{PBH}} \sim 0$ . From Eq. (5), under these conditions the inflaton will evolve as  $\ddot{\varphi} \approx -3H\dot{\varphi}$  and enter a phase of USR. This is illustrated in Fig. 2: when  $\varphi$  encounters the local feature in the potential, it slows down significantly;  $\epsilon$  correspondingly becomes small ( $\mathcal{O}(10^{-9})$ ), while  $\eta$  temporarily grows, surpassing the USR threshold of  $\eta = 3$ . In order for inflation to end, eventually seeding the conditions that could form today's Universe,  $\varphi$  needs to exit the USR phase and accelerate until  $\epsilon = 1$ .

For completeness we consider an alternative definition of the second slow-roll parameter, defined by

$$\epsilon_2 \equiv \frac{d \ln \epsilon}{dN} = \frac{\dot{\epsilon}}{H\epsilon}. \quad (11)$$

This is related to our definition of  $\eta$  by  $\epsilon_2 = -2\eta + 4\epsilon$ ; note that in the USR regime,  $\epsilon_2 \leq -6$ . We introduce the number of e-folds of expansion before the end of inflation,

$$N \equiv -\ln a, \quad dN = -d \ln a = H dt, \quad (12)$$

where  $N = 0$  at the end of inflation. In Fig. 2 and following, we adopt  $N$  as our time coordinate.

## B. Enter the spectator

We now turn back to the full form of Eq. (1), i.e. we add a spectator field  $\chi$  to the single-field model of Eq. (3). For concreteness, we continue to consider the potential  $V_{\text{PBH},A}$  of Eq. (4) in what follows. We shall assume the spectator is a free scalar field with mass  $m_\chi$  and potential given by  $V_S(\chi) = \frac{1}{2}m_\chi\chi^2$ .

We denote the inflaton-plus-spectator setup as ‘‘PBH-spec,’’ in contrast to the single-field or ‘‘SF’’ scenario. For

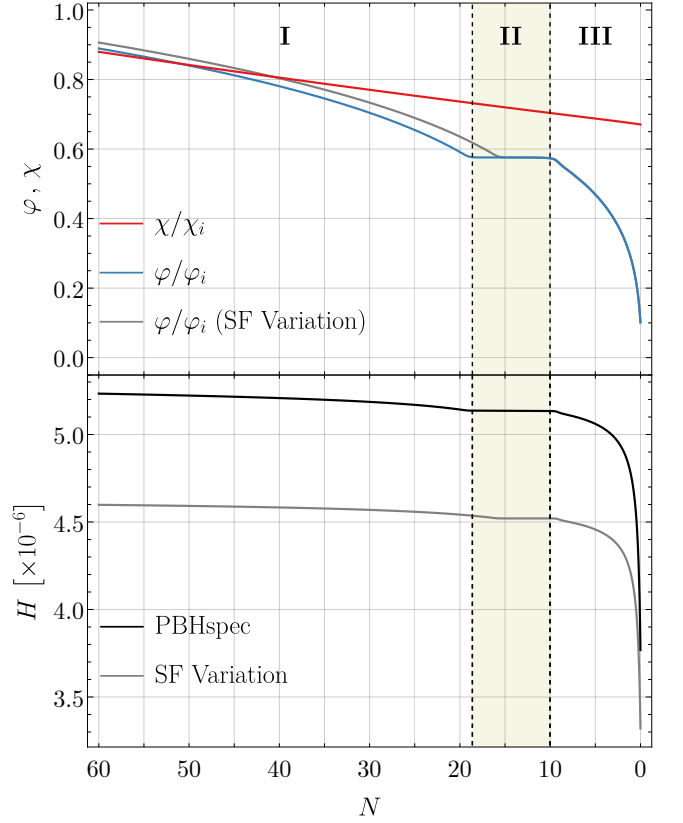


FIG. 3. Evolution of the background fields and the Hubble parameter (in units of  $M_{\text{Pl}}$ ) for the PBHspec model as compared to the single-field case, for fixed  $V_{\text{PBH},A}$  parameters (reported in Table I: ‘‘spectator’’ refers to the PBHspec model, ‘‘no spectator’’ refers to the Variation model). *Top panel:* The evolution of  $\varphi$  is similar to its single-field behaviour, slowing down when it hits the feature in  $V_{\text{PBH}}$  and slow-rolling elsewhere. The spectator field  $\chi$  slow-rolls at near-constant velocity, since  $V_S(\chi)$  does not exhibit any particular feature. *Bottom panel:* The Hubble parameter is increased with respect to its single-field value by the presence of  $\chi$ . This causes additional Hubble friction, which further slows down  $\varphi$ . *All panels:* The highlighted ‘phase II’ corresponds to the period of slower evolution of  $\varphi$ , encapsulating the single-field USR phase. As seen in Fig. 5, it is delimited by the turns in field space.

the PBHspec case, the background evolution of the fields is governed by their decoupled equations of motion,

$$\ddot{\varphi} + 3H\dot{\varphi} = -\partial_\varphi V_{\text{PBH}}, \quad \ddot{\chi} + 3H\dot{\chi} = -\partial_\chi V_S, \quad (13)$$

with  $\partial_\chi = \partial/\partial\chi$ , as well as one common Friedmann equation,

$$H^2 = \frac{1}{3M_{\text{Pl}}^2} \left( \frac{\dot{\varphi}^2}{2} + \frac{\dot{\chi}^2}{2} + V_{\text{PBH}} + V_S \right). \quad (14)$$

An *indirect coupling* between the two fields therefore emerges through their contributions to the Hubble parameter. Being subdominant,  $\chi$  causes a slight increase of  $H$ , therefore augmenting the Hubble friction of  $\varphi$  in Eq. (13).



Model	$V_0 [M_{\text{Pl}}^4]$	$\varphi_d [M_{\text{Pl}}]$	$m_\chi [M_{\text{Pl}}]$	$\chi_i [M_{\text{Pl}}]$
SF Reference	$7.2 \times 10^{-11}$	2.00	—	—
SF Variation	$6.5 \times 10^{-11}$	$2.00 \times (1 - 4 \times 10^{-4})$	—	—
PBHspec	$8.3 \times 10^{-11}$	$2.00 \times (1 - 4 \times 10^{-4})$	$6 \times 10^{-7}$	3

TABLE I. Parameter values for the PBHA models considered in this work. For the parameters of  $V_{\text{PBH},A}$  in Eq. (4), we fix the values  $M = 1/2$ ,  $A = 1.7373 \times 10^{-3}$ , and  $\sigma = 1.81 \times 10^{-2}$  (in units of  $M_{\text{Pl}}$ ) for each set of parameters, and always consider the inflaton initial value  $\varphi_i = 3.5 M_{\text{Pl}}$ . (The dynamics are nearly independent of  $\varphi_i$ , so long as it produces sufficient e-folds of inflationary expansion.) We set  $\dot{\varphi}_i = \dot{\chi}_i = 0$ . The single-field “Reference” model is defined so that it produces an enhancement of the curvature power spectrum consistent with PBH production, similarly to the baseline models considered in Refs. [48, 52]. The “Variation” model shifts the parameter  $\varphi_d \rightarrow \varphi_{d,\text{ref}} \times (1 - 4 \times 10^{-4})$ ; this excludes PBH production. The “PBHspec” model then adds a spectator field to the Variation model, keeping the  $V_{\text{PBH},A}$  parameters fixed (apart from the overall normalization scale  $V_0$ ). By including the spectator field, PBHspec allows for PBH production in the asteroid-mass range.

The evolution of the background fields and of the Hubble parameter, found by solving Eqs. (13)–(14), is shown in Fig. 3. The PBHspec scenario is compared to the single-field PBH model, for the same  $V_{\text{PBH},A}$  parameters (see “Variation” model in Table I; note this is not the same as the “Reference” parameters illustrated in Fig. 2). First, we note from the top panel that the evolution of  $\varphi$  (blue curve) is similar to its single-field behaviour (grey curve), insofar as it substantially slows down when  $\varphi$  encounters the feature in  $V_{\text{PBH}}(\varphi)$ : this corresponds to the single-field USR phase. The inflaton  $\varphi$  is slowed down for a longer period in the PBHspec case. Meanwhile, since  $V_S(\chi)$  has no special features, the spectator field  $\chi$  slow-rolls down its potential at a near-constant rate throughout the inflationary evolution. Correspondingly, the value of  $H$  is slightly increased throughout inflation by the presence of  $\chi$ ; most notably, the phase during which  $H$  “plateaus” is extended. This augments the Hubble friction that  $\varphi$  is subjected to, through Eq. (13), further slowing it down; this also explains why  $\varphi$  “plateaus” for a more extended period of time.

We introduce the usual multifield notation  $\phi^I = \{\varphi, \chi\}$ , where the index  $I$  spans over the number of fields; in the present scenario,  $I = 1, 2$ . (For a review of the formalism of multifield inflation see, e.g., Refs. [94–101].) The magnitude of the velocity of the background fields is given by

$$\dot{\sigma} \equiv |\dot{\phi}^I| = \sqrt{\dot{\varphi}^2 + \dot{\chi}^2}, \quad (15)$$

where the second equality is a consequence of the decoupling of the fields in our scenarios. Because of this decoupling, the first slow-roll parameter  $\epsilon$  of Eq. (7), which in a multifield scenario is given by  $\epsilon = \dot{\sigma}^2 / (2H^2 M_{\text{Pl}}^2)$ , becomes sum-separable:

$$\epsilon = \frac{1}{2} \frac{\dot{\varphi}^2}{H^2 M_{\text{Pl}}^2} + \frac{1}{2} \frac{\dot{\chi}^2}{H^2 M_{\text{Pl}}^2} \equiv \epsilon_\varphi + \epsilon_\chi. \quad (16)$$

Being an intrinsically multifield scenario, one must account for the possibility of turning field trajectories in field-space. We describe the direction of the background field system by defining the field-space unit vectors

$$\hat{\sigma}^I \equiv \frac{\dot{\phi}^I}{\dot{\sigma}} = \left\{ \frac{\sqrt{\epsilon_\varphi}}{\sqrt{\epsilon}}, \frac{\sqrt{\epsilon_\chi}}{\sqrt{\epsilon}} \right\}, \quad \hat{s}^J \equiv \varepsilon^{IJ} \hat{\sigma}_I. \quad (17)$$

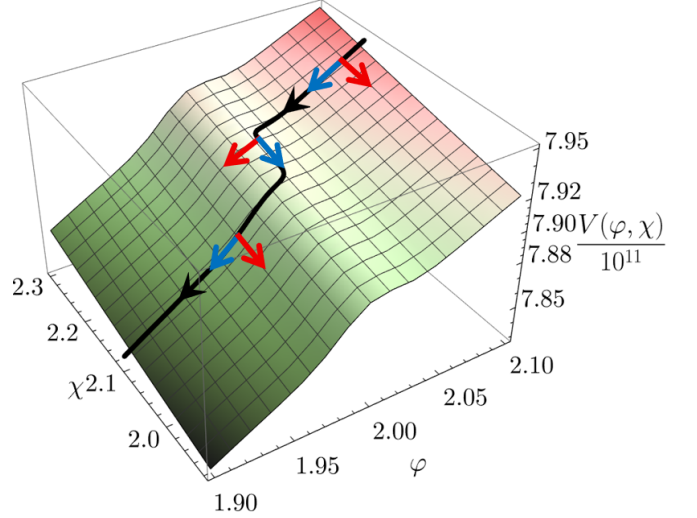


FIG. 4. Inflationary potential  $V(\varphi, \chi) = V_{\text{PBH},A}(\varphi) + V_S(\chi)$  (in units of  $M_{\text{Pl}}$ ), zoomed in on the region around the  $V_{\text{PBH},A}$  feature (corresponding to the inset in Fig. 1). The trajectory of the background field system is superimposed (black curve), as well as the direction of  $\hat{\sigma}^I$  (blue) and  $\hat{s}^I$  (red) at three points of the inflationary evolution corresponding to phases I–III. The “bump” along the  $\varphi$  direction causes the trajectory to temporarily turn from the  $\varphi$  direction to the  $\chi$  direction; during this phase,  $\hat{\sigma}^I$  and  $\hat{s}^I$  switch roles. The PBHspec parameter values are listed in Table I.

The former points along the direction of the fields’ motion (called the *adiabatic* or *curvature* direction), while the latter is orthogonal to it (the *entropy* or *isocurvature* direction). In Eq. (17),  $\varepsilon^{IJ}$  is the two-dimensional, anti-symmetric Levi-Civita pseudo-tensor. Lastly, we define the turn rate pseudo-vector and pseudo-scalar,

$$\omega^I \equiv \partial_t \hat{\sigma}^I, \quad \omega \equiv \varepsilon_{IJ} \hat{\sigma}^I \omega^J, \quad (18)$$

which describe the time evolution of the fields’ trajectory in field space. In the setup of Eq. (1), the turn rate simplifies to  $\omega = \dot{\theta}$  where  $\theta$  is the angle between  $\hat{\sigma}^I$  and the  $\varphi$ -axis.

The field-space trajectory of the  $V_{\text{PBH},A}$  model is illustrated in Fig. 4, superimposed onto the two-field potential of Eq. (2). This trajectory exhibits two turns,

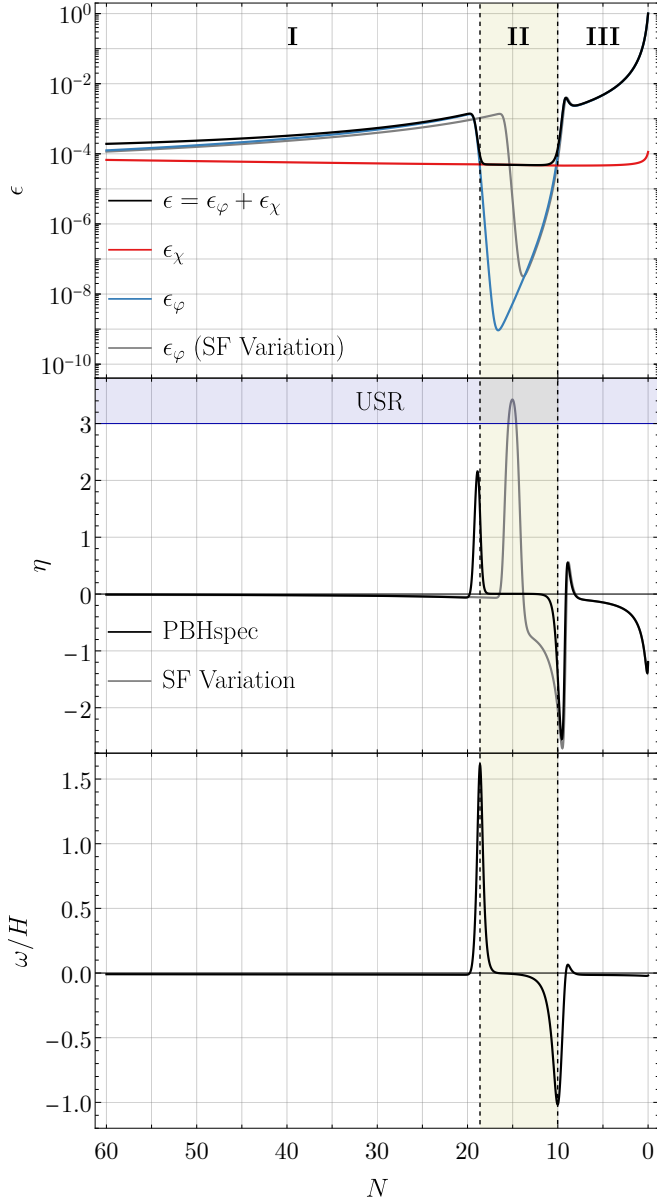


FIG. 5. Evolution of the slow-roll parameters and the turn rate for the PBHspec and single-field models considered in Fig. 3 (parameter values reported in Table I). *Top panel:* The presence of  $\chi$  sets a floor on  $\epsilon \geq \epsilon_\chi$ : while  $\epsilon_\phi$  becomes small (tracing the single-field case),  $\epsilon_\chi \sim 10^{-4}$  and we never see  $\epsilon \rightarrow 0$ . *Middle panel:* As  $\epsilon$  never becomes unusually small,  $\eta$  never enters the USR regime (unlike the single-field case). *Bottom panel:* The trajectory of the background fields exhibits two turns, corresponding to the transitions between  $\epsilon \approx \epsilon_\phi$  and  $\epsilon \approx \epsilon_\chi$  (and vice-versa). *All panels:* The highlighted ‘phase II’ is delimited by the turns in field space (the dashed vertical lines correspond to the extrema of  $\omega$ ). During this phase,  $\epsilon_\chi \gg \epsilon_\phi$ .

taking place when the field system reaches the feature in  $V_{\text{PBH},A}$ : when the inflaton  $\phi$  slows down, the small but steady evolution of the spectator field  $\chi$  becomes important, inducing the trajectory to temporarily turn along

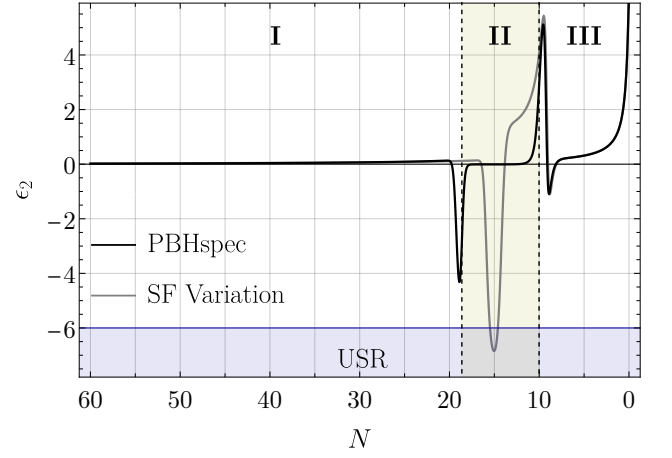


FIG. 6. Evolution of the  $\epsilon_2$  slow-roll parameter, Eq. (11), for the same models considered in Figs. 3–5. Consistent with the middle panel of the latter figure, we can see here that the PBHspec model never enters ultra-slow-roll, whereas the single-field model spends  $\sim \mathcal{O}(1)$  efold within USR.

the  $\chi$  direction until  $\phi$  accelerates again. The unit vector  $\hat{\sigma}^I$  (in blue, at different stages of the inflationary evolution) traces the direction of the trajectory, while  $\hat{s}^I$  (in red) is orthogonal to it.

Fig. 5 shows the evolution of the slow-roll parameters and of the turn rate, for the PBHspec scenario as compared to the single-field PBH model. The same parameters as in Fig. 3 are considered here.

From the evolution of  $\epsilon$  (top panel), we note that the sum-separability of Eq. (16) means that the presence of  $\chi$  sets a *floor* on the total  $\epsilon$ , which can never be smaller than  $\epsilon \approx \epsilon_\chi$ . While  $\epsilon_\phi$  reaches values of  $\mathcal{O}(10^{-9})$ , similarly to the single-field case (although it dips lower than the dashed-gray curve, due to the additional Hubble friction provided by  $\chi$ ),  $\epsilon_\chi$  never departs from slow-roll and is near-constant at  $\sim \mathcal{O}(10^{-4})$ . The first slow-roll parameter is therefore bounded by  $\epsilon \geq \epsilon_\chi$ . As shown in the middle panel of Fig. 5, by incorporating the decoupled spectator field, the system *never enters USR*: even when  $\phi$  slows significantly, the system’s velocity along the  $\chi$  direction prevents the system from entering ultra-slow-roll, with  $\eta < 3$  at all times.

Lastly, we confirm from the plot of  $\omega$  (bottom panel of Fig. 5) that two turns take place. Interestingly, these correspond to the beginning and end of the phase in which  $\epsilon_\phi$  becomes very small and  $\epsilon$  is bounded from below by  $\epsilon_\chi$ , denoted by “phase II.” This can be understood by looking at the form of the adiabatic unit vector  $\hat{\sigma}^I$  of Eq. (17). During the first phase of inflation,  $\epsilon_\phi > \epsilon_\chi$  and  $\hat{\sigma}^I$  predominantly points along the  $\phi$  direction. When  $\phi$  slows down and  $\epsilon_\phi$  decreases, we rapidly find  $\epsilon_\chi \gg \epsilon_\phi$  and  $\hat{\sigma}^I$  turns to point along the  $\chi$  direction. Once  $\phi$  exits the feature in  $V_{\text{PBH}}$ , it quickly accelerates and we return to the regime  $\epsilon_\phi > \epsilon_\chi$ :  $\hat{\sigma}^I$  thus turns back to point along the  $\phi$  direction. Note that  $\chi$  never accelerates: its near-constant velocity, subdominant during phases I and III,

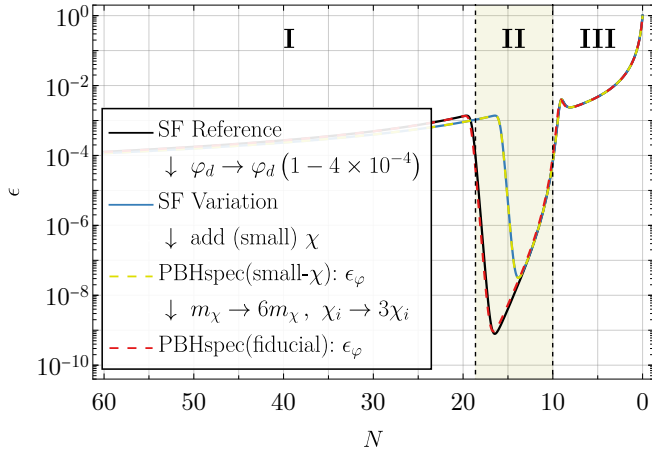


FIG. 7. Evolution of the inflaton’s slow-roll parameter  $\epsilon_\varphi$  in the single-field and PBHspec models, and parameter compensations. In the single-field model, a small variation  $\varphi_d \rightarrow (1 - 4 \times 10^{-4})\varphi_d$  drastically modifies the dynamics (black to blue curve). When a spectator field is present, this shift can be compensated by  $\mathcal{O}(1)$  variations in the spectator field’s parameters (yellow-dashed to red-dashed).

becomes relevant when  $\varphi$  decelerates sufficiently. Only during the brief phase II does  $\chi$  temporarily dominate the evolution of the system.

For completeness, we also show in Fig. 6 the evolution of the  $\epsilon_2$  slow-roll parameter of Eq. (11), for the same parameter sets considered above. This clearly matches the behaviour of  $\eta$ : the single-field model enters a short phase of ultra-slow-roll (defined here as  $\epsilon_2 \leq -6$ ), while the PBHspec scenario is prevented from entering this regime. We also point out that the spectator field’s relative contribution to the energy density of the Universe is subdominant throughout the inflationary evolution,  $\rho_\chi/\rho_{\text{tot}} \lesssim 0.02$ .

### C. Relisience to parameter variations

The addition of the spectator field endows the PBH model with a *resilience* to parameter variations. This can be observed already at the background level, from the evolution of  $\epsilon_\varphi$ . In Fig. 7 we compare  $\epsilon$  in the single-field case to  $\epsilon_\varphi$  in the PBHspec model. The black curve depicts  $\epsilon$  for the single-field “Reference” model of Table I, protagonist of Section II A and consistent with PBH production: as noted previously,  $\epsilon$  decreases to  $\mathcal{O}(10^{-9})$ . Through a tiny variation in one of the  $V_{\text{PBH},A}$  parameters,  $\varphi_d \rightarrow \varphi_d(1 - 4 \times 10^{-4})$ , the black curve is shifted to the blue curve (“Variation” model of Table I). The evolution of  $\epsilon$  is changed dramatically, still supporting a phase of USR (gray curve in Fig. 5) but not sufficient to produce PBHs.

Adding a spectator field to the single-field Variation model may not change the situation (blue to yellow-dashed), but making the spectator more massive can re-

store  $\epsilon_\varphi$  to its original form (yellow-dashed to red-dashed:  $m_\chi \rightarrow 6m_\chi$ ,  $\chi_i \rightarrow 3\chi_i$ ) *without* requiring any fine-tuning beyond  $\mathcal{O}(1)$  changes. The evolution of  $\epsilon_\varphi$  is therefore resilient to small variations in the  $V_{\text{PBH}}$  parameters, due to compensations by the spectator field.

## III. PERTURBATIONS

We now consider perturbations to the background system, using the familiar multifield formalism of Refs. [94–101]. Throughout the classical evolution of the background fields described in the previous section, quantum fluctuations will be sourced. At any point in space and time, each field can be expanded around its homogeneous background value,

$$\Phi^I(x^\mu) = \phi^I(t) + \delta\phi^I(x^\mu), \quad (19)$$

where  $\phi^I = \{\varphi, \chi\}$  obey Eq. (13) and  $\delta\phi^I$  represent small departures from the background value. Considering perturbations around flat Friedmann-Lemaître-Robertson-Walker spacetimes, one may construct the Mukhanov-Sasaki variables, which remain gauge-invariant to first order in the perturbations,

$$Q^I \equiv \delta\phi^I + \frac{\dot{\phi}^I}{H}\psi, \quad (20)$$

where  $\psi(x^\mu)$  is the comoving scalar metric perturbation on equal-time hypersurfaces.

The PBHspec setup discussed in Section II B is intrinsically multifield. Having multiple possible directions in field space, quantum fluctuations will be produced both *along* the direction of the background fields’ motion, and *perpendicular* to it. These correspond to the adiabatic and isocurvature directions identified in Eq. (17). The Mukhanov-Sasaki variables of Eq. (20) can then be projected along the field-space unit-vectors as

$$Q^I = \hat{\sigma}^I Q_\sigma + \hat{s}^I Q_s, \quad (21)$$

thus defining the scalar adiabatic and isocurvature perturbations  $Q_\sigma$  and  $Q_s$ , respectively. These can be recast as the canonically normalized comoving perturbations

$$\mathcal{R} = \frac{H}{\dot{\sigma}} Q_\sigma, \quad (22)$$

$$\mathcal{S} = \frac{H}{\dot{\sigma}} Q_s. \quad (23)$$

The adiabatic (or curvature) perturbation  $\mathcal{R}$  is also produced in single-field inflationary models, while the isocurvature perturbation  $\mathcal{S}$  is unique to multifield systems. Whereas the former reflects variations in the total energy density of the Universe, the latter leaves the total energy density unchanged while modifying the ratio of energy density associated with distinct particle species at various spacetime locations.

The power spectra for the curvature and isocurvature perturbations are defined as the two-point correlators

$$\mathcal{P}_{\mathcal{X}}(k, N) \equiv \frac{k^3}{2\pi^2} |\mathcal{X}_k(N)|^2, \quad (24)$$

for  $\mathcal{X} = \{\mathcal{R}, \mathcal{S}\}$ . When the time dependence is not explicitly stated, the power spectrum will be evaluated at the end of inflation,  $\mathcal{P}_{\mathcal{X}}(k) \equiv \mathcal{P}_{\mathcal{X}}(k, N_{\text{end}})$ . This is the principal quantity of interest for studying predictions from inflation, as its shape can be tested against observational data, as discussed further in Section IV C.

### A. Single-field ultra-slow-roll

In the single-field model described in Section II A, the Mukhanov-Sasaki variable of Eq. (21) reduces to the scalar perturbation along the trajectory of the inflaton,  $Q_{\sigma}$ . The curvature perturbation satisfies

$$\mathcal{R} \equiv \frac{H}{\dot{\varphi}} Q_{\sigma} = \frac{H}{\dot{\varphi}} \delta\varphi + \psi. \quad (25)$$

It can be decomposed into Fourier modes  $\mathcal{R}_k$ , which cross the Hubble radius  $(aH)^{-1}$  at a time  $N_*$  where the comoving wavenumber  $k = a(N_*)H(N_*)$ . To linear order in the perturbations, these modes obey the equation of motion

$$\ddot{\mathcal{R}}_k + (3 + \delta)H\dot{\mathcal{R}}_k + \frac{k^2}{a^2}\mathcal{R}_k = 0, \quad (26)$$

where we use the notation  $\delta = \epsilon_2 = 4\epsilon - 2\eta$  for consistency with the literature. In the limit  $k \ll aH$ , curvature perturbations will be enhanced whenever the Hubble damping term  $(3 + \delta)H\dot{\mathcal{R}}_k$  becomes negative. A phase of ultra-slow-roll, as defined by Eq. (10), provides exactly these conditions. In particular, whenever  $\epsilon \ll 1$  and  $\eta \geq 3/2$ , long-wavelength modes for which  $k^2/(aH)^2 < |\dot{\mathcal{R}}_k/(H\mathcal{R}_k)|$  will be *anti-damped*, growing quasi-exponentially.

This behaviour can be seen in Fig. 8 for the single-field  $V_{\text{PBH},A}$  potential of Eq. (4): when the system enters the phase of ultra-slow-roll (top panel,  $\eta \geq 3$ ), the curvature perturbation grows quasi-exponentially (bottom panel), resulting in an enhancement of  $\sim 10^6$  with respect to its pre-USR values. Notice that the figure portrays the evolution of the time-dependent power spectrum for a fixed  $k$ -mode. The curvature mode shown here crosses the Hubble radius shortly before the onset of the USR phase, thus simultaneously satisfying the condition for anti-damping and being subjected to the entirety of the USR-induced growth. It thus corresponds to the mode  $\mathcal{R}_{k_{\text{peak}}}$ , which is maximally enhanced.

### B. Influence of the Spectator

Curvature perturbations are always produced during the inflationary expansion. Additionally, the presence of

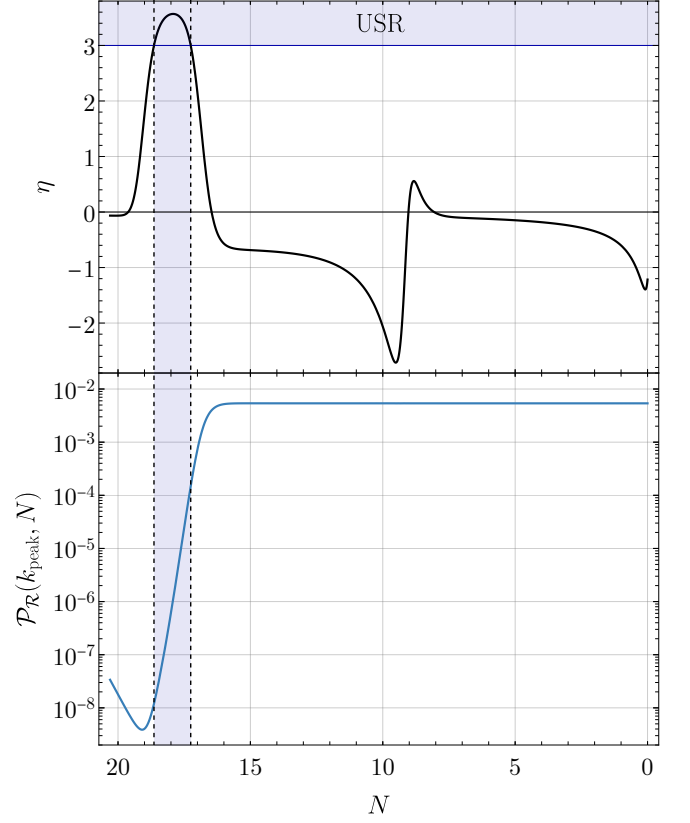


FIG. 8. Evolution of the second slow-roll parameter  $\eta$  and corresponding amplification of the curvature mode  $\mathcal{R}_{k_{\text{peak}}}$ , in the single-field “Reference” model of Table I. *Top panel:* As seen previously in Fig. 2,  $\eta$  crosses the USR threshold for  $\sim 1.4$  e-folds, inducing a phase of ultra-slow-roll evolution. *Bottom panel:* We depict the time-dependent power spectrum for a curvature mode  $\mathcal{R}_{k_{\text{peak}}}$  that exits the Hubble radius shortly before the onset of the USR phase (at  $N_* \approx 18$ ). While  $\eta \geq 3/2$ , the curvature perturbation grows, with  $\mathcal{P}_{\mathcal{R}}(k_{\text{peak}}, N)$  being enhanced by  $\sim 10^6$ . After USR, the curvature mode remains frozen at this enhanced value until the end of inflation.

the spectator field makes it possible for the isocurvature fluctuations of Eq. (23) to be produced as well. The equations of motion for the Fourier modes of these two types of perturbations are coupled. To linear order, they obey

$$\frac{d}{dt} (\dot{\mathcal{R}}_k - 2\omega \mathcal{S}_k) + (3 + \delta)H (\dot{\mathcal{R}}_k - 2\omega \mathcal{S}_k) + \frac{k^2}{a^2} \mathcal{R}_k = 0, \quad (27)$$

$$\ddot{\mathcal{S}}_k + (3 + \delta)H\dot{\mathcal{S}}_k + \left( \frac{k^2}{a^2} + \mu_s^2 \right) \mathcal{S}_k = -2\omega \dot{\mathcal{R}}_k. \quad (28)$$

We define the effective isocurvature mass as

$$\mu_s^2 = \mathcal{M}_{ss} - \mathcal{M}_{\sigma\sigma} + 2H^2\epsilon(3 + \delta - \epsilon), \quad (29)$$

with  $\mathcal{M}_{\sigma\sigma}$  and  $\mathcal{M}_{ss}$  being the projections of the mass-matrix  $\mathcal{M}_J^I = \partial^I \partial_J V$  along the adiabatic and isocurva-



ture directions, respectively:<sup>2</sup>

$$\mathcal{M}_{\sigma\sigma} = \hat{\sigma}^I \hat{\sigma}^J \partial_I \partial_J V, \quad (30)$$

$$\mathcal{M}_{ss} = \hat{s}^I \hat{s}^J \partial_I \partial_J V, \quad (31)$$

with  $\partial_I V \equiv \partial V / \partial \phi^I$ .

In the long-wavelength limit, that is, on super-Hubble scales ( $k/a \ll H$ ), the equations of motion of Eqs. (27)–(28) simplify to

$$\dot{\mathcal{R}}_k \simeq 2\omega \mathcal{S}_k, \quad (32)$$

$$\ddot{\mathcal{S}}_k + (3 + \delta)H\dot{\mathcal{S}}_k + \tilde{\mu}_s^2 \mathcal{S}_k \simeq 0, \quad (33)$$

with the effective isocurvature mass defined as  $\tilde{\mu}_s^2 \equiv \mu_s^2 + 4\omega^2$ . The equation of motion for  $\mathcal{S}_k$  indicates that isocurvature modes will be enhanced whenever  $\tilde{\mu}_s^2 < 0$ , corresponding to a phase of tachyonic instability, and they will decay whenever  $\tilde{\mu}_s^2 > 0$ . The evolution of  $\mathcal{R}_k$ , meanwhile, indicates that there can be a super-Hubble transfer of power from isocurvature to curvature perturbations whenever the background fields' trajectory experiences a turn in field-space, with  $\omega \neq 0$ .

In the PBHspec model of Eq. (1), the USR enhancement of curvature modes is supplanted by a transient period of tachyonic isocurvature growth and a subsequent transfer of power to curvature modes. After the first turn in field space, when  $\epsilon_\chi \gg \epsilon_\varphi$ , the adiabatic unit vector  $\hat{\sigma}^I$  will temporarily point along the  $\chi$  direction and, vice-versa, the isocurvature vector  $\hat{s}^I$  will trace the  $\varphi$  direction. For this reason, within phase II, the mass-matrix projections become  $\mathcal{M}_{\sigma\sigma} \approx \partial_\chi^2 V_S(\chi)$  and  $\mathcal{M}_{ss} \approx \partial_\varphi^2 V_{\text{PBH}}(\varphi)$ . The effective isocurvature mass then simplifies to

$$\mu_s^2 \approx \partial_\varphi^2 V_{\text{PBH}}(\varphi) - \partial_\chi^2 V_S(\chi), \quad (34)$$

since the last term in Eq. (29) is suppressed by  $\epsilon$ . The second term in Eq. (34) is negative definite since the spectator field's mass must be a real quantity. As mentioned at the end of Section II B, the first term necessarily becomes temporarily negative in order for  $\varphi$  to evolve beyond the local feature in  $V_{\text{PBH}}$ , and for inflation to end. This indicates that during most of phase II,  $\mu_s^2$  is negative, indicating a tachyonic instability of the isocurvature perturbations.

We can indeed observe a tachyonic instability when examining the evolution of  $\mu_s^2$  for  $V_{\text{PBH},A}$  of Eq. (4), as shown in the top panel of Fig. 9.<sup>3</sup>

<sup>2</sup> Given our simple setup, with strictly canonical kinetic terms for both fields and hence a trivial field-space structure, the effective masses  $\mathcal{M}_{\sigma\sigma}$  and  $\mathcal{M}_{ss}$  do not involve any terms related to the (here vanishing) Riemann tensor of the field-space manifold. For the more general case, see, e.g., Ref. [100].

<sup>3</sup> Note that we consider the evolution of  $\mu_s^2$  instead of the super-Hubble mass  $\tilde{\mu}_s^2$  introduced in Eq. (33), because the  $k$ -modes analyzed here only exit the Hubble radius at the time of the first turn. Given that  $k/a \sim H$  at those times, the effective mass  $\mu_s^2$  of Eq. (29) remains most relevant. Shortly thereafter, though, the regime  $k/a \ll H$  becomes valid, and for most of phases II and III, these modes evolve with  $\tilde{\mu}_s^2 \simeq \mu_s^2$ , as shown in Fig. 12.

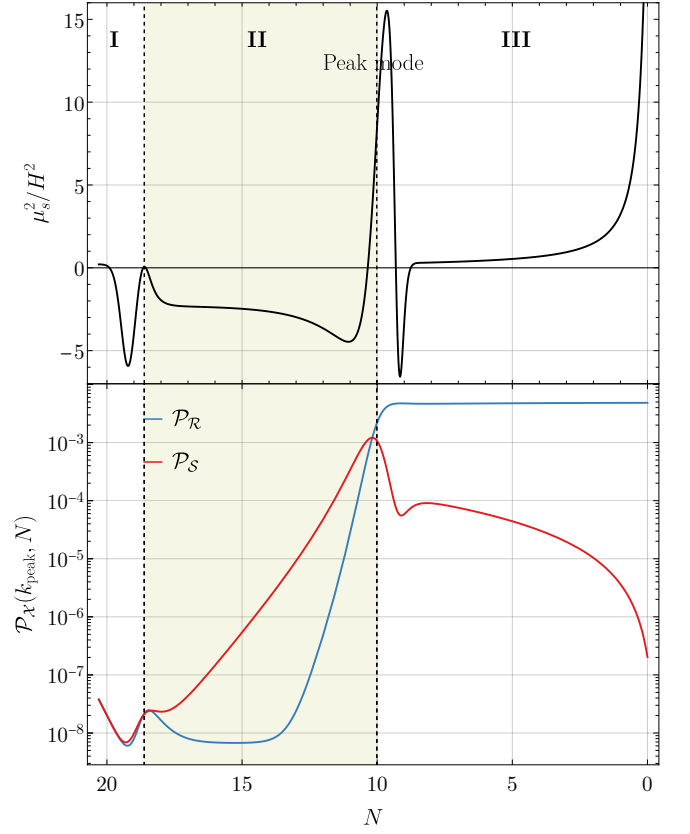


FIG. 9. Evolution of the effective isocurvature mass  $\mu_s^2$  and interaction of the curvature and isocurvature perturbations  $\mathcal{R}_{k_{\text{peak}}}$  and  $\mathcal{S}_{k_{\text{peak}}}$  for the PBHspec model. *Top panel:* During phase II (when  $\epsilon_\chi \gg \epsilon_\varphi$  and the system evolves along the  $\chi$  direction),  $\mu_s^2$  becomes negative: the isocurvature perturbations experience a tachyonic instability. Toward the end of inflation,  $\mu_s^2$  becomes large and positive. *Bottom panel:* The time-dependent power spectra for curvature  $\mathcal{R}_{k_{\text{peak}}}$  and isocurvature  $\mathcal{S}_{k_{\text{peak}}}$  modes that exit the Hubble radius shortly before the beginning of phase II, that is, just before the first turn in field space (at  $N_* \approx 18$ ). The tachyonic phase causes a near-exponential growth of  $\mathcal{S}_k$ , which then transfers its power to  $\mathcal{R}_k$  at the end of phase II, when the second turn takes place. During phase III, the positive  $\mu_s^2$  causes  $\mathcal{S}_k$  to decay.

Correspondingly, isocurvature modes  $\mathcal{S}_k$  experience a rapid growth during phase II (bottom panel, red curve). They then transfer their power to  $\mathcal{R}_k$  (blue curve) during the second turn in field space, at the interface between phases II and III. Afterwards,  $\mathcal{S}_k$  modes quickly decay due to  $\mu_s^2$  becoming large and positive, while modes  $\mathcal{R}_k$  instead become frozen at their amplified value.

### C. Common ground

Both the single-field and PBHspec models show an enhancement of perturbations, though by means of totally different mechanisms. It is helpful to pause and consider the relation between the two models.

To understand the mapping between the single-field and PBHspec model, consider the equations of motion for the field fluctuations, namely the gauge invariant Mukhanov-Sasaki variables of Eq. (21). Denoting the perturbations  $Q^I = \{Q_\varphi, Q_\chi\}$ , we note that these are related to  $Q_\sigma, Q_s$  by a time-dependent rotation defined by the direction of  $\hat{\sigma}^I$ . Let us compare the single-field USR phase with the PBHspec phase II, when  $\omega = 0$  and the crucial growth of isocurvature occurs.

In the single-field case,  $Q_\sigma = Q_\varphi$ , which evolves following [100]

$$\ddot{Q}_\varphi + 3H\dot{Q}_\varphi + \left[ \frac{k^2}{a^2} + \mathcal{M}_{\sigma\sigma} - \frac{1}{M_{\text{Pl}}^2 a^3} \frac{d}{dt} \left( \frac{a^3 \dot{\varphi}^2}{H} \right) \right] Q_\varphi = 0. \quad (35)$$

The third term in the brackets is suppressed by  $\epsilon$ , which is exponentially small during the single-field USR phase. Since  $\mathcal{M}_{\sigma\sigma} = \partial_\varphi^2 V_{\text{PBH}}$  in this scenario, we can therefore approximate Eq. (35) as

$$\ddot{Q}_\varphi + 3H\dot{Q}_\varphi + \left[ \frac{k^2}{a^2} + \partial_\varphi^2 V_{\text{PBH}}(\varphi) \right] Q_\varphi \approx 0. \quad (36)$$

In the PBHspec case, one has both  $Q_\sigma$  and  $Q_s$ . We are especially interested in the latter, which evolves as [100, 102, 103]

$$\ddot{Q}_s + 3H\dot{Q}_s + \left[ \frac{k^2}{a^2} + \mathcal{M}_{ss} + 3\omega^2 \right] Q_s = 4M_{\text{Pl}}^2 \frac{\omega}{\dot{\sigma}} \frac{k^2}{a^2} \psi. \quad (37)$$

During phase II, while  $\hat{\sigma}^I$  is aligned with the  $\chi$  direction, one has  $Q_s \approx Q_\varphi$  and  $\mathcal{M}_{ss} \approx \partial_\varphi^2 V_{\text{PBH}}$ . Since  $\omega = 0$  during this phase, Eq. (37) takes the simple form

$$\ddot{Q}_\varphi + 3H\dot{Q}_\varphi + \left[ \frac{k^2}{a^2} + \partial_\varphi^2 V_{\text{PBH}}(\varphi) \right] Q_\varphi \approx 0, \quad (38)$$

which exactly matches the equation for  $Q_\varphi$  in the single-field model, Eq. (36). Both are completely determined by  $H$  and  $\partial_\varphi^2 V_{\text{PBH}}$ , and in particular, we expect the evolution to be completely described by the evolution of the dimensionless ratio  $\partial_\varphi^2 V_{\text{PBH}}/H^2$ . To make this more explicit, we rewrite Eq. (38) by changing variables from cosmic time to number of e-folds (see Eq. (12); primes denote  $N$ -derivatives) and dividing by  $H^2$ :

$$Q_\varphi'' + (3 - \epsilon) Q_\varphi' + \left[ \frac{k^2}{(aH)^2} + \frac{\partial_\varphi^2 V_{\text{PBH}}(\varphi)}{H^2} \right] Q_\varphi \approx 0. \quad (39)$$

The quantity  $\partial_\varphi^2 V_{\text{PBH}}/H^2$  will therefore act as a mass term for the evolution of  $Q_\varphi$ . On super-Hubble scales, when  $k/(aH) \ll 1$ , this equation will display the same behaviour as Eq. (33): we expect  $Q_\varphi$  to grow when  $\partial_\varphi^2 V_{\text{PBH}}/H^2 < 0$ , and to decay when  $\partial_\varphi^2 V_{\text{PBH}}/H^2 > 0$ . In Fig. 10 we compare the evolution of  $\partial_\varphi^2 V_{\text{PBH}}/H^2$  in the single-field model and in the PBHspec model.

This establishes a correspondence between the growth of perturbations in the two models. In the single-field

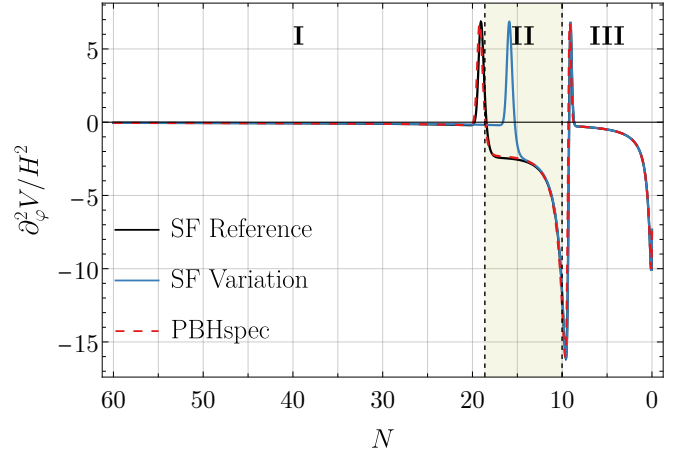


FIG. 10. Evolution of  $\partial_\varphi^2 V/H^2$ . This quantity determines the USR growth of the single-field PBH model and the tachyonic growth of isocurvature perturbations in the PBHspec model. The former relies on a finely-tuned feature of the potential, whereas the latter does not.

case, the growth is attributed to ultra-slow-roll evolution while the field traverses a fine-tuned feature of its potential. In the PBHspec scenario, this is realized as a tachyonic growth of isocurvature perturbations, which can then transfer power to the curvature perturbations during a field-space turn. Importantly, the latter is realized *without the need to fine-tune the potential*.

#### IV. POWER SPECTRUM AND CMB OBSERVABLES

We numerically solve the background equations of Eqs. (13)–(14) and perturbation equations of Eqs. (27)–(28), with Bunch-Davies initial conditions imposed on the perturbations. We perform the calculations of both background quantities and perturbations using two independent codes written in Python and Mathematica, respectively, and find excellent agreement between the two. In Python, we use the publicly available code `PyTransport` [104, 105], which uses the Transport Method [106] to directly compute the time-evolution of correlation functions. In Mathematica, we solve the perturbation equations in the form presented in Ref. [107] and, from this, construct the power spectra.

The power spectrum of curvature perturbations  $\mathcal{P}_{\mathcal{R}}(k)$  for the PBHspec model is shown in Figure 11. In this section we analyze this power spectrum in detail, separating our discussion into the modes relevant to PBH formation and those relevant to CMB observations.

##### A. Shape of the Power Spectrum

As we have seen in Section III, the dynamics of the single-field and PBHspec models produce an amplifica-

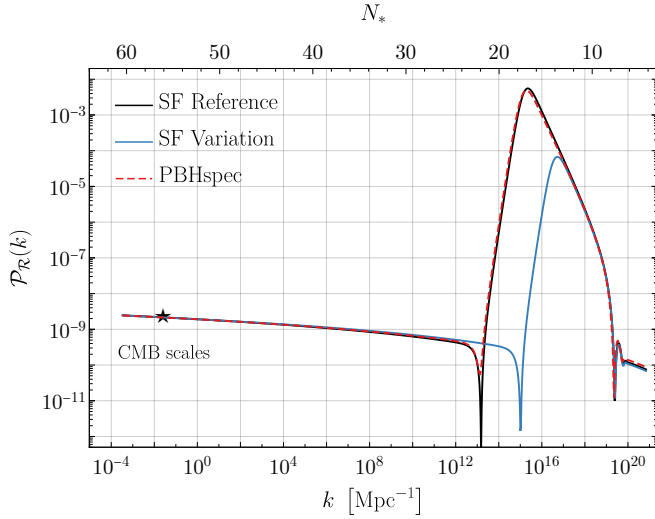


FIG. 11. Power spectrum of curvature perturbations for the  $V_{\text{PBH,A}}$  potential of Eq. (4), in both the single-field (black and blue curves) and PBHspec (red curve) scenarios. The parameters used in the Figure are summarized in Table I. The black and red curves exhibit a large (and similar) enhancement of  $\mathcal{P}_{\mathcal{R}}$ , albeit due to different mechanisms; as the peak of these spectra surpasses the threshold of  $10^{-3}$ , these models allow for the production of primordial black holes. These models satisfy the “steepest growth” constraints [108], as  $\mathcal{P}_{\mathcal{R}} \propto k^4$  to the left of the peak, and the CMB parametrization  $\mathcal{P}_{\mathcal{R}} = A_s(k/k_{\text{CMB}})^{n_s-1}$  at the CMB parametrization highlighted by the black star.

tion of the curvature perturbations for certain “peak”  $k$ -modes, albeit through very different mechanisms. This leads to an enhancement of the curvature power spectrum on a characteristic scale  $k$  set by the timing of the onset of the USR (single-field) or tachyonic (PBHspec) phase. This is illustrated in Fig. 11, in which we show the curvature power spectrum for varying  $k$  evaluated at the end of inflation.

One may appreciate that the characteristic peak of  $\mathcal{P}_{\mathcal{R}}(k)$  in the PBHspec scenario (red curve) closely mirrors the single-field result (black and blue curves), even though the multifield PBHspec system never enters a phase of USR. To the left of the peak, the spectrum realizes the well-studied “steepest growth,” with  $\mathcal{P}_{\mathcal{R}}(k) \propto k^4$  [108]. To the right of the peak, the spectrum features a sharp decay (which is a power law for constant- $\eta$  models [51]). The peak of the power spectrum is realized by the modes which exit the Hubble radius shortly before or during phase II, analogous to the single-field scenario in which the peak is due to modes that exit at the onset of the USR phase.

To understand the emergence of the peak in the spectrum, it is useful to contrast the peak modes with modes that exit the horizon much earlier than the first turn in field space. Here there is a key consideration: the effective isocurvature mass is different for sub-Hubble and super-Hubble modes. In particular, the super-Hubble

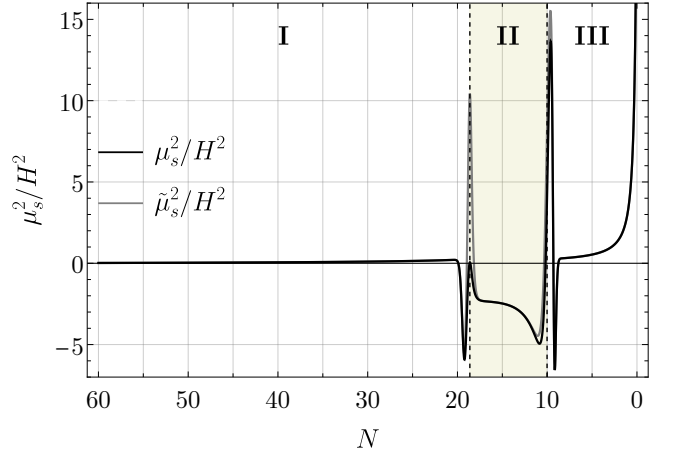


FIG. 12. Evolution of the effective isocurvature mass for sub-Hubble ( $\mu_s^2$ ) and super-Hubble ( $\tilde{\mu}_s^2$ ) modes, for the PBHspec model of  $V_{\text{PBH,A}}$ . The two quantities differ by  $4\omega^2$ , which becomes significant during the transitions between different phases. Most remarkably, at the transition between phases I and II,  $\tilde{\mu}_s^2$  gains a substantial contribution from the turn. As  $\tilde{\mu}_s^2$  becomes large and positive, it causes isocurvature modes that are already super-Hubble at this time to be largely suppressed. The tachyonic instability is near-identical for the two quantities, meaning all  $\mathcal{S}_k$  modes experience a similar tachyonic growth during phase II, and eventually decay during phase III.

mass,  $\tilde{\mu}_s^2$ , gains an additional term  $4\omega^2$ . The effective isocurvature mass is shown in Fig. 12, where black and grey correspond to sub- and super-Hubble modes, respectively. One can appreciate from this that modes which are already super-Hubble at the onset of phase II will experience a brief period of superheavy mass:  $\tilde{\mu}_s^2/H^2$  spikes up to  $\mathcal{O}(10)$ . This causes isocurvature modes that are already super-Hubble at that time to be suppressed, before the start of the phase II tachyonic instability. This behaviour is illustrated in Fig. 13 for modes which exit the Hubble radius at CMB scales. Similarly, modes that become super-Hubble in phase III, after the tachyonic instability, have predominantly heavy isocurvature mass, resulting in negligible growth (and then decay) of isocurvature perturbations.

Additionally, the peak modes—as opposed to modes on scales relevant to CMB measurements—only satisfy  $k < aH$  during one turn in field space (the second one). This causes a positive transfer of power from the enhanced  $\mathcal{S}_k$  to the  $\mathcal{R}_k$  modes at the end of phase II, as was previously observed in Fig. 9. On the other hand, CMB modes (and any  $k$ -mode that is super-Hubble at the onset of phase II) satisfy  $k \ll aH$  during two opposing turns in field space. As can be appreciated from Fig. 13, the first turn induces a positive transfer of power from  $\mathcal{S}_k$  to  $\mathcal{R}_k$ , while the second one—being of opposite sign—induces a *negative* transfer from  $\mathcal{S}_k$  to  $\mathcal{R}_k$ . The curvature perturbations  $\mathcal{R}_k$  on such scales are therefore decreased by the second turn, reducing them near-exactly to their phase I values.

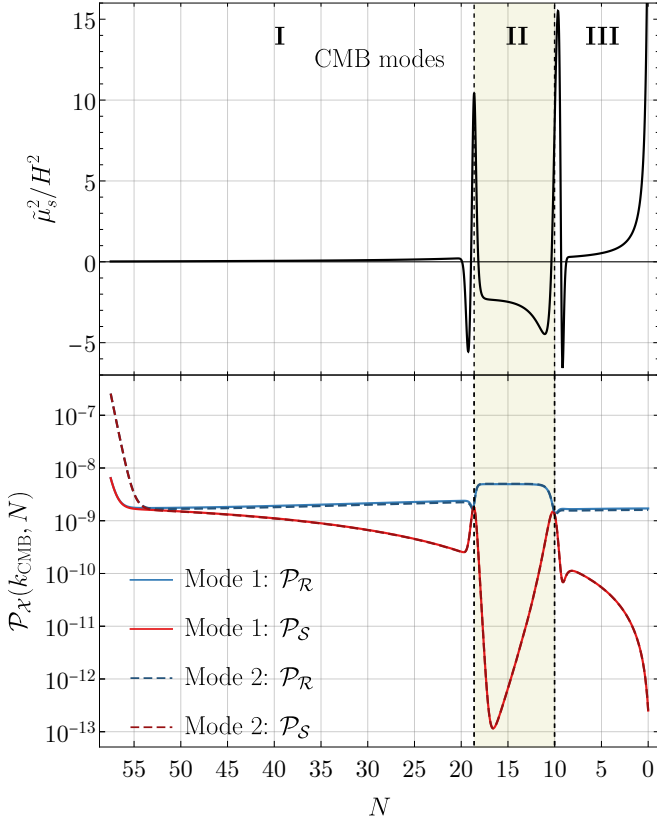


FIG. 13. Evolution of the super-Hubble effective isocurvature mass  $\tilde{\mu}_s^2$  and the curvature and isocurvature perturbations  $\mathcal{R}_k$  and  $\mathcal{S}_k$ , for two  $k$ -modes that cross the Hubble radius around CMB scales, near  $k_{\text{CMB}} = 0.05 \text{ Mpc}^{-1}$ . *Top panel:* At the boundary between phases I and II,  $\tilde{\mu}_s^2$  briefly becomes large and positive due to the presence of a turn in field space. During phase II (when  $\epsilon_\chi \gg \epsilon_\phi$  and the system evolves along the  $\chi$  direction),  $\tilde{\mu}_s^2$  drives a tachyonic instability for modes  $\mathcal{S}_k$ , while in phase III it grows to become large and positive. *Bottom panel:* The time-dependent power spectra of Eq. (24), for the curvature and isocurvature perturbations of two modes  $k_{\text{CMB},1}$  and  $k_{\text{CMB},2}$  that cross the Hubble radius 2 e-folds apart, at CMB scales. Before exhibiting the tachyonic growth of phase II (similarly to the “peak” modes of Fig. 9) and the late-time decay of phase III, CMB modes are suppressed by  $\sim \mathcal{O}(10^{-4})$  between phases I and II. This is due to the positive peak of  $\tilde{\mu}_s^2$ , which affects the evolution of modes near  $k_{\text{CMB}}$  but which occurs while modes with  $k_{\text{peak}} \gg k_{\text{CMB}}$  remain deep inside the Hubble radius. The sharp peak of  $\tilde{\mu}_s^2$  therefore compensates the tachyonic enhancement for modes near  $k_{\text{CMB}}$ , but not for those near  $k_{\text{peak}}$ . Furthermore, the two opposing field-space turns that occur while the modes with  $k_{\text{CMB}}$  are outside the Hubble radius cause two transfers of power from  $\mathcal{S}_k$  to  $\mathcal{R}_k$ : the first one is positive, while the second is negative. The value of  $\mathcal{P}_\mathcal{R}(k_{\text{CMB}})$  at the end of inflation is therefore near-identical to its single-field value when CMB modes first cross the Hubble radius (explaining the similarity in  $A_s$ ). Furthermore, the evolution of  $k_{\text{CMB},1}$  and  $k_{\text{CMB},2}$  is self-similar, explaining why the values of  $n_s$  (and  $\alpha_s$ ) are similar to the single-field model.

In sum, these effects lead to the characteristic peak

structure of the curvature power spectrum, in which the enhanced modes become amplified by the transfer of power from the tachyonic growth of isocurvature modes identified in the previous section.

## B. Primordial Black Holes

Primordial black holes are formed through the gravitational collapse of large overdensities after the end of inflation. For such overdensities to be produced, the inflationary curvature power spectrum needs to be enhanced by  $\mathcal{O}(10^6)$  with respect to its CMB scales, while remaining within the perturbative regime. A power spectrum which exhibits a peak with  $10^{-3} \leq \mathcal{P}_\mathcal{R}(k_{\text{peak}}) \ll 1$  will therefore support PBH production [14, 109–113].

In the PBHspec model, the peak of the power spectrum occurs at the mode  $k_{\text{peak}}$  which exits the horizon shortly before the onset of phase II. This maps onto the typical mass of the produced primordial black holes (that is, the mass at the peak of the PBH mass distribution [29]) in an identical manner to the single-field case, as

$$\frac{M_{\text{PBH},f}}{30 M_\odot} \approx \left(\frac{\gamma}{0.2}\right) \left(\frac{g_*(T_f)}{106.75}\right)^{-\frac{1}{6}} \left(\frac{k_{\text{peak}}}{3.2 \times 10^5 \text{ Mpc}^{-1}}\right)^{-2}, \quad (40)$$

where  $M_{\text{PBH},f}$  is the PBH mass at the time of its formation [51]. We take the efficiency factor  $\gamma = 0.2$  [5] and consider the effective number of degrees of freedom to be  $g_*(T_f) = 106.75$  at the time of formation; the solar mass is  $M_\odot \approx 2.0 \times 10^{33} \text{ g}$ . From this, we find that the power spectrum in Fig. 11 yields primordial black holes with typical mass  $5.9 \times 10^{19}$ , which is within the asteroid mass range,  $10^{17} \text{ g} \leq M_{\text{PBH}} \leq 10^{23} \text{ g}$  [8–17].

## C. CMB Observables

A remarkable feature of the PBHspec scenario is that it preserves the CMB predictions of the single-field model. The CMB observables for all the models considered in this work are summarized in Table II.

Modes that correspond to the comoving CMB pivot scale  $k_{\text{CMB}} = 0.05 \text{ Mpc}^{-1}$  exit the Hubble radius at a time [114, 115]

$$N_{\text{CMB}} \simeq 62 + \frac{1}{4} \ln \left( \frac{\rho_{\text{CMB}}^2}{3M_{\text{Pl}}^6 H_e^2} \right) + \frac{1 - 3w_{\text{reh}}}{12(1 + w_{\text{reh}})} \ln \left( \frac{\rho_{\text{rad}}}{\rho_e} \right) \simeq 56 \pm 5$$

before the end of inflation. Here  $\rho_{\text{CMB}}$  is the energy density of the Universe at the time  $N_{\text{CMB}}$ , while  $\rho_{\text{rad}}$  is the value at the onset of radiation-domination [116–119]; the quantities  $H_e$  and  $\rho_e$  are calculated at the end of inflation. The equation of state during reheating falls within the range  $\omega_{\text{reh}} \in \{-1/3, +1\}$ : the result  $N_{\text{CMB}} = 56$  in Eq. (41) assumes instantaneous reheating ( $\omega_{\text{reh}} =$

Model	$A_s$	$n_s$	$\alpha_s$	$r$	$\beta_{\text{iso}}$	$f_{\text{NL}}^{\text{ortho}}$	$M_{\text{PBH}} [\text{g}]$	$V_S/V_{\text{PBH}}$	$m_\chi/H$
SF Reference	$2.11 \times 10^{-9}$	0.9678	$-6.8 \times 10^{-4}$	0.002	—	0.25	$1.0 \times 10^{15}$	—	—
SF Variation	$2.10 \times 10^{-9}$	0.9698	$-6.0 \times 10^{-4}$	0.002	—	0.25	—	—	—
PBHspec	$2.10 \times 10^{-9}$	0.9685	$-6.4 \times 10^{-4}$	0.003	$1.5 \times 10^{-4}$	0.25	$5.9 \times 10^{19}$	0.01	0.12

TABLE II. Observables for the parameter sets considered for the PBHA model (as defined in Table I). CMB scales exit at  $N_{\text{CMB}} = 56$ . The non-Gaussianities are peaked in the orthogonal configuration, and  $\beta_{\text{iso}}$  is taken at the scale  $k = 0.05 \text{ Mpc}^{-1}$  (i.e.,  $k_{\text{mid}}$  in Ref [63]). We evaluate the ‘spectator-ness’ measures  $V_S/V_{\text{PBH}}$  and  $m_\chi/H$  at  $N_{\text{CMB}}$ . Observables are computed using PyTransport.

1/3), and the range  $\pm 5$  comes from the uncertainty in the duration of the phase of reheating [116].

We parametrize the primordial power spectrum of curvature perturbations  $\mathcal{P}_{\mathcal{R}}(k)$  on CMB scales via the conventional form [120]

$$\mathcal{P}_{\mathcal{R}}(k) \equiv A_s \left( \frac{k}{k_{\text{CMB}}} \right)^{n_s - 1 + \frac{1}{2} \alpha_s \ln \left( \frac{k}{k_{\text{CMB}}} \right)}, \quad (41)$$

where  $A_s = \mathcal{P}_{\mathcal{R}}(k_{\text{CMB}})$  is the amplitude at the CMB pivot scale,  $n_s$  is the spectral index, and  $\alpha_s$  is the running of the spectral index. The latter are defined as

$$n_s \equiv 1 + \left. \frac{d \ln \mathcal{P}_{\mathcal{R}}(k)}{d \ln k} \right|_{k=k_{\text{CMB}}}, \quad (42)$$

$$\alpha_s \equiv \left. \frac{d n_s}{d \ln k} \right|_{k=k_{\text{CMB}}}. \quad (43)$$

We also define the tensor-to-scalar ratio  $r$  as the ratio between the amplitudes of tensor and scalar (curvature plus isocurvature) perturbations at the CMB pivot scale,

$$r \equiv \left. \frac{\mathcal{P}_t(k)}{\mathcal{P}_{\mathcal{R}}(k) + \mathcal{P}_{\mathcal{S}}(k)} \right|_{k=k_{\text{CMB}}}. \quad (44)$$

The primordial isocurvature fraction is defined as [63]

$$\beta_{\text{iso}}(k) \equiv \frac{\mathcal{P}_{\mathcal{S}}(k)}{\mathcal{P}_{\mathcal{R}}(k) + \mathcal{P}_{\mathcal{S}}(k)}, \quad (45)$$

which we evaluate at the CMB pivot scale, corresponding to the scale  $k_{\text{mid}}$  in Ref. [63]. Constraints on these quantities are summarized in Table III.

Parameter	Constraint
$A_s [\times 10^{-9}]$	$2.10 \pm 0.03$
$n_s$	$0.9665 \pm 0.0038$
$\alpha_s$	$-0.0045 \pm 0.0067$
$r$	$< 0.037$
$\beta_{\text{iso}}$	$< 0.001$

TABLE III. Parameter constraints for CMB observables from Planck 2018 CMB data [62–64]. For  $\beta_{\text{iso}}$ , we adopt the most conservative constraint on the isocurvature fraction at the CMB pivot scale from Table 14 of [63].

As discussed in the previous section, the CMB-scale modes do not experience a significant enhancement in the

PBHspec scenario. This results in an overall preservation of the single-field predictions for the CMB.

The presence of the spectator field may rescale the amplitude  $A_s$  by  $\mathcal{O}(0.1 - 1)$  with respect to its single-field values. This effect is due to a partial compensation between the turns into and out of phase II, and is completely degenerate with the normalization of the potential. An  $\mathcal{O}(1)$  change in the  $V_{\text{PBH},A}$  parameter  $V_0$  can thus keep the PBHspec model consistent with CMB constraints.

Crucially, nearby  $k$ -modes on CMB scales experience a near-identical change in amplitude, resulting in a negligible change to  $n_s$ . To demonstrate this explicitly, we show in Fig. 13 the evolution of two neighboring  $k$ -modes exiting the Hubble radius around CMB scales (two e-folds apart). One may see that the two  $k$ -modes experience identical evolution during phase II. In particular, the small difference between the amplitudes of  $\mathcal{R}_k$  for the two modes is maintained to sub-percent precision between early times ( $N \sim 40$ , long before the phase II mechanism has an impact on the dynamics) and the end of inflation ( $N = 0$ , after the phase II dynamics). The same reasoning also explains the small change in  $\alpha_s$ .

The isocurvature fraction  $\beta_{\text{iso}}$  may also be read off from Fig. 13, from the relative size of  $\mathcal{P}_{\mathcal{S}}$  and  $\mathcal{P}_{\mathcal{R}}$  at the end of inflation. From this we find  $\beta_{\text{iso}} = 1.5 \times 10^{-4}$ , well below the CMB constraint.

Meanwhile, the tensor modes are not impacted at all by the spectator dynamics. The spectrum of tensor modes is given by  $\mathcal{P}_t = H^2(N_{\text{CMB}})/(8\pi^2 M_{\text{Pl}}^2)$ , from which we infer  $r = 8\pi^2 A_s/H^2(N_{\text{CMB}}) = 3 \times 10^{-3}$ , essentially unchanged from the single-field model.

#### D. Non-Gaussianity

Finally, we examine the non-Gaussianity of the PBHspec model. That is, we investigate how the curvature perturbations produced in this setup depart from a Gaussian distribution, as probed by the three-point correlator,

$$\langle \mathcal{R}_{\mathbf{k}_1} \mathcal{R}_{\mathbf{k}_2} \mathcal{R}_{\mathbf{k}_3} \rangle \equiv (2\pi)^3 \delta^3(\mathbf{k}_1 + \mathbf{k}_2 + \mathbf{k}_3) B_{\mathcal{R}}(k_1, k_2, k_3), \quad (46)$$

which defines the bispectrum  $B_{\mathcal{R}}(k_1, k_2, k_3)$  for three  $k$ -modes which form a closed triangle in Fourier space,  $\mathbf{k}_1 + \mathbf{k}_2 + \mathbf{k}_3 = 0$ . It is useful to define the reduced bispectrum,



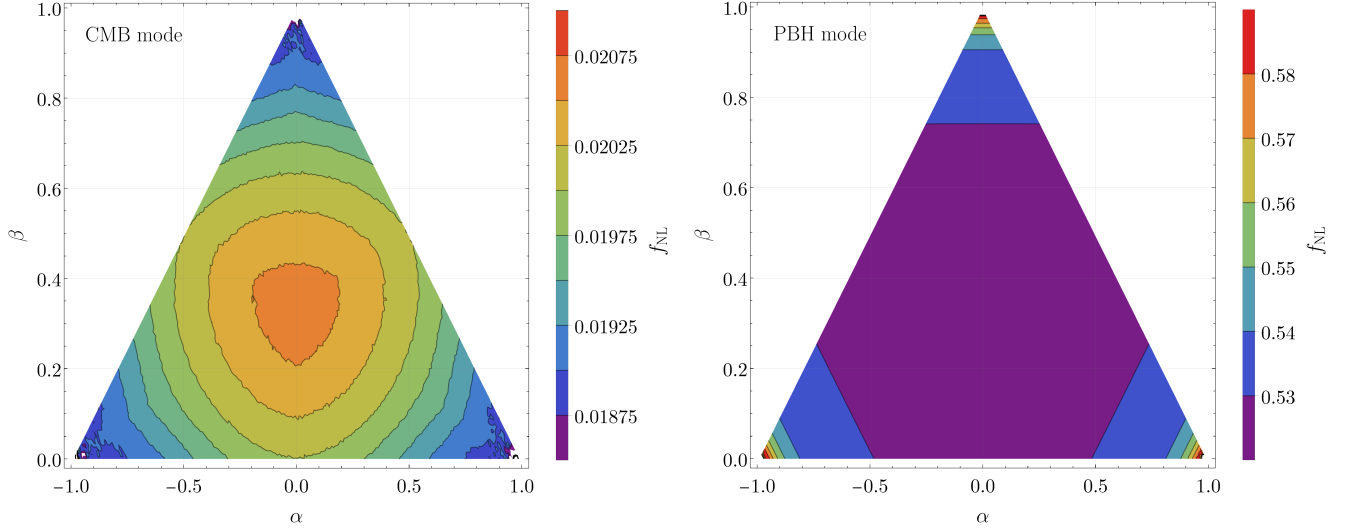


FIG. 14. Reduced bispectrum of curvature perturbations, projected onto the  $\alpha - \beta$  plane for fixed  $k$ -modes, evaluated at the end of inflation. We find the non-Gaussianity is near-constant across all shapes, with a shape-dependence that is much smaller than the experimental sensitivity to non-Gaussianity. *Left panel:*  $f_{\text{NL}}$  on CMB scales. Non-Gaussianities are slightly peaked in the equilateral configuration, with  $f_{\text{NL}}^{\text{equil}} = 0.02$ , and are consistent with the CMB constraints of Table IV. *Right-panel:*  $f_{\text{NL}}$  on PBH scales ( $k = k_{\text{peak}}$ ). Non-Gaussianities are enhanced with respect to CMB scales, being peaked in the local configuration with  $f_{\text{NL}}^{\text{local}} = 0.6$ . The presence of significant non-Gaussianity at these scales may assist the formation of primordial black holes.

or non-Gaussianity parameter [121],

$$f_{\text{NL}} \equiv \frac{5}{6} \frac{B_{\mathcal{R}}(k_1, k_2, k_3)}{P_{\mathcal{R}}(k_1)P_{\mathcal{R}}(k_2) + P_{\mathcal{R}}(k_2)P_{\mathcal{R}}(k_3) + P_{\mathcal{R}}(k_1)P_{\mathcal{R}}(k_3)} \quad (47)$$

where  $P_{\mathcal{R}}(k) = 2\pi^2 \mathcal{P}_{\mathcal{R}}(k)/k^3$  is the dimensionful power spectrum.

To determine the shape of the non-Gaussianity and in which configuration it is peaked, we adopt the  $\alpha - \beta$  formalism of Refs. [122, 123]. This defines the variables

$$\alpha = \frac{k_2 - k_3}{k}, \quad \beta = \frac{k - k_1}{k}, \quad \text{with } k = \frac{k_1 + k_2 + k_3}{2}, \quad (48)$$

where  $0 \leq \beta \leq 1$  and  $-(1-\beta) \leq \alpha \leq 1-\beta$ . As illustrated in Fig. 14, the bispectrum can be projected onto the  $\alpha - \beta$  plane, forming a triangle. The center of the triangle corresponds to the equilateral configuration ( $k_1 = k_2 = k_3$ ), its corners represent the squeezed (or local) limit ( $k_1 \ll k_2 = k_3$ ), and the middle of the sides indicate the orthogonal configuration ( $k_1 = 2k_2 = 2k_3$ ).

We first calculate the non-Gaussianity for modes that cross the Hubble radius at CMB scales. The projection of  $f_{\text{NL}}$  onto the  $\alpha - \beta$  plane is illustrated in the left panel of Fig. 14. The values of  $f_{\text{NL}}$  in each configuration can be read off from the figure, corresponding to

$$f_{\text{NL}}^{\text{local}} = 0.01, \quad f_{\text{NL}}^{\text{equil}} = 0.02, \quad f_{\text{NL}}^{\text{ortho}} = 0.02. \quad (49)$$

The non-Gaussianity on CMB scales is weakly peaked in the equilateral configuration, with each component sitting well below the CMB bounds summarized in Table IV. Interestingly, these values are very similar to those

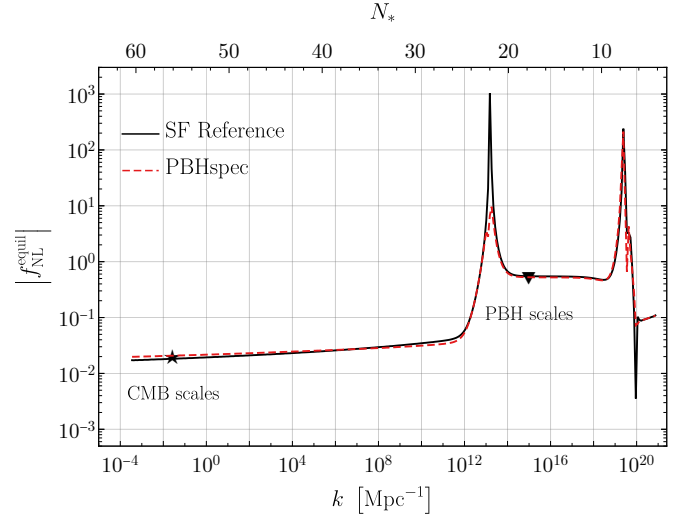


FIG. 15. Amplitude of the equilateral configuration of the non-Gaussianity,  $f_{\text{NL}}^{\text{equil}}$ , for modes that exit the Hubble radius at different times during inflation. The star and triangle indicate CMB and PBH scales, respectively. The single-field and PBHspec models have small and near-identical non-Gaussianity at CMB scales, which is significantly enhanced on PBH scales, where the PBHspec scenario shows a slightly smaller  $f_{\text{NL}}$  than the single field model.

in the single-field model. This can be understood by the fact that  $k$ -modes exiting around CMB scales are only modestly impacted by the tachyonic instability of the isocurvature modes, thus reproducing the single-field results.

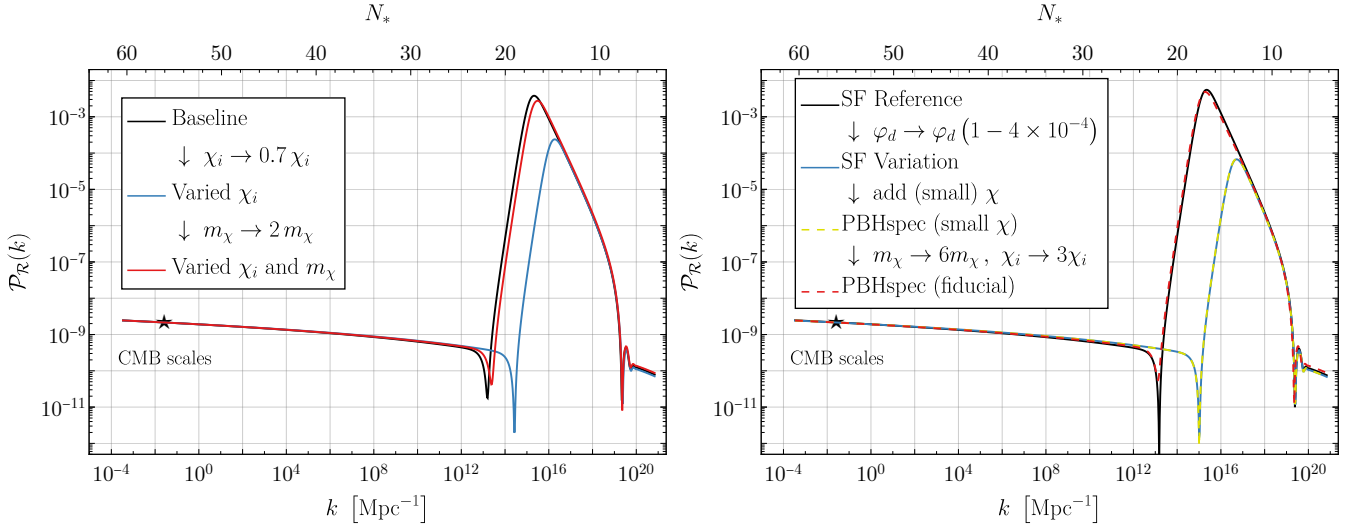


FIG. 16. Parameter dependence of the curvature power spectrum for the PBHspec model. The base model PBHA of Eq. (4) is adopted for illustrative purposes. *Left panel:* Dependence of the model on  $\mathcal{O}(1)$  variations in the spectator parameters, producing  $\mathcal{O}(10)$  shifts in the amplitude of the peak of  $\mathcal{P}_{\mathcal{R}}$  (black to blue and blue to red), and partial compensation between the shifts in  $m_\chi$  and  $\chi_i$  (black to red). The PBH parameters for all the curves are fixed to their fiducial values as reported in the PBHspec row of Table I, with the “baseline” model having  $m_\chi = 3.5 \times 10^{-7} M_{\text{Pl}}$  and  $\chi_i = 4 M_{\text{Pl}}$ ; the corresponding observables are consistent with those described in Table II. *Right panel:* Dependence of the single-field model on a  $\mathcal{O}(10^{-4})$  variation in the inflaton parameter  $\varphi_d$ , producing an  $\mathcal{O}(10)$  shift in the amplitude of the peak of  $\mathcal{P}_{\mathcal{R}}$  (black to blue). Null effect of adding a small spectator field to the system (blue to yellow-dashed), and compensation of the previous shift by  $\mathcal{O}(1)$  variations in the spectator parameters (yellow-dashed to red-dashed). The model parameters used here are reported in Table I.

Parameter	Constraint
$f_{\text{NL}}^{\text{local}}$	$-0.9 \pm 5.1$
$f_{\text{NL}}^{\text{equil}}$	$-26 \pm 47$
$f_{\text{NL}}^{\text{ortho}}$	$-38 \pm 24$

TABLE IV. Parameter constraints for the non-Gaussianity parameter  $f_{\text{NL}}$  from Planck 2018 CMB data [61].

The right panel of Fig. 14 shows the  $\alpha - \beta$  projection of the non-Gaussianity for modes exiting the Hubble radius at PBH scales. One may appreciate an enhancement of the non-Gaussianity for these modes, leading to  $f_{\text{NL}} \sim 0.5$ . This is peaked in the equilateral configuration, and is similar to the single-field model.

To understand the scale dependence of the non-Gaussianity, in Fig. 15 we plot  $f_{\text{NL}}^{\text{equil}}$  as a function of wavenumber  $k$ . From this, one may appreciate the dramatic enhancement of non-Gaussianity on small scales around the PBH scale. In this case, we also include the single-field PBH model for reference. The non-Gaussianity of PBH modes is, in fact, much lower in the spectator case than in the single field case. This can be attributed to the reduction of  $|\eta|$  in the PBHspec scenario as compared to the single-field case.

## V. PARAMETER DEPENDENCE

The spectator sector of the model of Eq. (1) depends only on two parameters: the field’s mass,  $m_\chi$ , and its initial value,  $\chi_i$ . An  $\mathcal{O}(1)$  variation in either parameter can produce  $\sim \mathcal{O}(10)$  shifts in the peak amplitude of  $\mathcal{P}_{\mathcal{R}}$ , which is significant but modest in comparison to the sensitivity of the single-field model to variations in the parameters of  $V_{\text{PBH}}$ . An example of this dependence is illustrated in the left panel of Fig. 16: varying  $\chi_i \rightarrow 0.7\chi_i$  can decrease the peak of  $\mathcal{P}_{\mathcal{R}}(k)$  by  $\mathcal{O}(10)$  (black to blue curve), and shifting  $m_\chi \rightarrow 2m_\chi$  can increase it by a similar amount (blue to red). Since these shifts compensate each other, one may also appreciate a partial degeneracy in  $m_\chi$  and  $\chi_i$ . This can be physically understood in terms of their combined contribution to the Hubble parameter and to the slow-roll parameter  $\epsilon_\chi$ .

On the other hand, the inflaton sector of the model is highly dependent on parameter variations. It is well known that the issue of fine-tuning plagues single-field inflationary models that produce PBHs through a phase of USR [52]. Indeed, predictions for observables in such models are exponentially sensitive to small variations their model parameters: a delicate balance needs to be struck to produce an appropriate abundance of PBHs (of the correct mass) while also satisfying high-precision CMB constraints. This is shown in the right panel of Fig. 16: a small variation (of  $\mathcal{O}(10^{-4})$ ) in the PBHA model parameter  $\varphi_d$  shifts the peak amplitude of the cur-

vature power spectrum by  $\mathcal{O}(10)$ , from  $\mathcal{P}_{\mathcal{R}} \sim \text{few} \times 10^{-3}$  (black curve; consistent with PBH production) to  $\mathcal{P}_{\mathcal{R}} \lesssim 10^{-4}$  (blue curve; too low to produce PBHs).

These two contrasting trends indicate that the spectator-plus-inflaton system retains a certain *resilience* to small variations in the PBH model parameters. In the illustrative example of Fig. 16 (right panel), the above-mentioned  $\mathcal{O}(10)$  shift in the peak amplitude of  $\mathcal{P}_{\mathcal{R}}$  due to the small PBH parameter variation (black to blue curve) can be compensated by a  $\mathcal{O}(1)$  variation in the spectator parameters (yellow-dashed to red-dashed curve). The compensated model (red) is consistent with the initial one (black) and compatible with PBH production in the asteroid-mass range, as well as with all CMB constraints.

This significant resilience of the model to small parameter variations suggests that fine-tuning of the single-field model may be ameliorated. To quantify this statement, we perform a Markov Chain Monte Carlo analysis of the single-field and spectator models fit to CMB data under the prior of asteroid-mass PBH dark matter, and compute the Bayesian evidence. This will be presented elsewhere [124].

## VI. MODEL (IN)DEPENDENCE

In the previous sections, we took the inflaton potential to follow the particular form of Eq. (4) for the sake of clarity. However, the mechanism we present is strongly model-independent: any potential  $V_{\text{PBH}}(\varphi)$  that produces PBHs through a transient phase of ultra-slow-roll (when treated as a single-field model) would be similarly affected by the presence of a spectator. This is due to two reasons.

In any such model, a light spectator field can easily realize an  $\epsilon_{\chi}$  larger than  $\epsilon_{\varphi}$  when  $\varphi$  slows down (causing  $\epsilon_{\varphi}$  to become small). This will produce two opposite turns in field space, delimiting a phase wherein the field trajectory is aligned with the  $\chi$  direction (our “phase II”).

Additionally, the presence of a local USR-inducing feature in  $V_{\text{PBH}}$  requires  $\partial_{\varphi} V_{\text{PBH}} \sim 0$ . In order for  $\varphi$  to eventually escape the USR feature and terminate inflation, the potential must (briefly) obey  $\partial_{\varphi}^2 V_{\text{PBH}} < 0$  during phase II. The latter condition *necessarily* causes  $\mu_s^2$  to temporarily become negative when the field trajectory is aligned with the  $\chi$  direction, sourcing a tachyonic growth of isocurvature perturbations. These will enhance the curvature modes when the second turn occurs, at the end of phase II.

To demonstrate this point, we calculate the evolution of the background fields and their perturbations for a second single-field model that can produce PBHs:

$$V_{\text{PBH},B}(\varphi) = \frac{M_{\text{Pl}}^4 \lambda v^4 x^2 (6 - 4ax + 3x^2)}{12 (M_{\text{Pl}}^2 + bx^2)^2}, \quad (50)$$

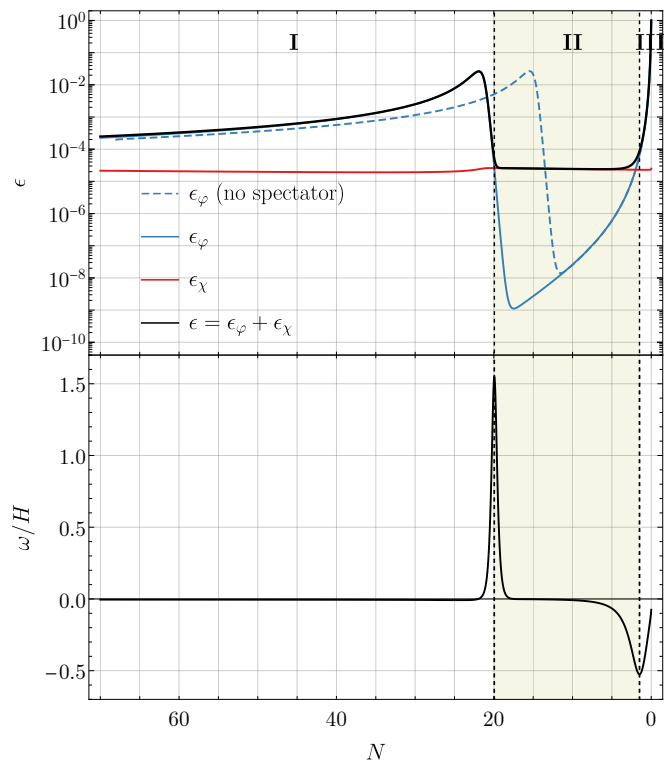


FIG. 17. Evolution of  $\epsilon$  and  $\omega$  in the PBHspec scenario, for the  $V_{\text{PBH},B}$  potential of Eq. (50). The parameters used in the Figure are summarized in Table V.

with  $x \equiv \varphi/v$ . This is the model developed in Refs. [39, 40], in which a cubic term is added to a Higgs-like potential [125] to engineer a local USR-inducing quasi-inflection point.

Note that, apart from exhibiting a local feature that slows down the evolution of  $\varphi$ , the potentials  $V_{\text{PBH},A}$  of Eq. (4) and  $V_{\text{PBH},B}$  of Eq. (50) do not have much in common. They are in fact derived from different considerations and use different sets of parameters.

The evolution of the background quantities  $\epsilon$  and  $\omega$  for the potential  $V_{\text{PBH},B}$  of Eq. (50) is shown in Fig. 17. The same behaviour previously encountered in Fig. 5 can be found here: the presence of the spectator field  $\chi$  sets a floor on  $\epsilon$ , and causes two turns in field space while eliminating the phase of ultra-slow-roll.

The corresponding evolution of the curvature and isocurvature perturbations is illustrated in Fig. 18. Here again, we find a tachyonic instability of  $\mu_s^2$  during phase II: this sources a near-exponential growth of modes  $\mathcal{S}_k$ , which then transfers power to modes  $\mathcal{R}_k$  at the time of the second turn in field space. The curvature power spectrum is thus enhanced, as shown in Fig. 19.

One may notice that phase II lasts longer in the PBHB model than in PBHA, while phase III is shortened. We can expect additional modes to cross the Hubble radius during phase II and experience the tachyonic enhancement, while only a few will exit during phase III. These considerations will affect the shape of the peak of the cur-

Model	$\lambda$	$v$ [ $M_{\text{Pl}}$ ]	$m_\chi$ [ $M_{\text{Pl}}$ ]	$\chi_i$ [ $M_{\text{Pl}}$ ]
SF Reference	$1.16 \times 10^{-6}$	0.19669	—	—
SF Variation	$9.10 \times 10^{-7}$	$0.19669 \times (1 - 4 \times 10^{-3})$	—	—
PBHspec	$1.19 \times 10^{-6}$	$0.19669 \times (1 - 4 \times 10^{-3})$	$7 \times 10^{-7}$	2.5

TABLE V. Parameter values for the PBHB models, with  $a = 0.719527$ ,  $b = 1.500016$ , and  $\varphi_i = 3 M_{\text{Pl}}$  fixed throughout (we take  $\dot{\varphi}_i = \dot{\chi}_i = 0$ ). The single-field “Reference” model reproduces the results introduced in Ref. [39], modified to align with the latest CMB constraints and produce PBHs in the asteroid-mass range. The “Variation” model shifts the parameter  $v \rightarrow v_{\text{ref}} \times (1 - 4 \times 10^{-3})$ ; this excludes PBH production. The “PBHspec” model includes the effect of a spectator field to the “Variation”  $V_{\text{PBH},B}$  parameters; it is again consistent with PBH production in the asteroid-mass range.

Model	$A_s$	$n_s$	$\alpha_s$	$r$	$\beta_{\text{iso}}$	$f_{\text{NL}}^{\text{ortho}}$	$M_{\text{PBH}}$ [g]	$R_V$	$m_\chi/H$
Reference	$2.10 \times 10^{-9}$	0.9599	$-1.8 \times 10^{-3}$	0.005	—	0.66	$1.1 \times 10^{17}$	—	—
Variation	$2.10 \times 10^{-9}$	0.9665	$-8.2 \times 10^{-4}$	0.004	—	0.66	—	—	—
PBHspec	$2.09 \times 10^{-9}$	0.9640	$-1.0 \times 10^{-3}$	0.005	$2.9 \times 10^{-4}$	0.66	$4.0 \times 10^{16}$	0.008	0.10

TABLE VI. Observables for the parameter sets considered for the PBHB model (as defined in Table V). CMB scales exit at  $N_{\text{CMB}} = 56$ . The non-Gaussianities are peaked in the orthogonal configuration, and  $\beta_{\text{iso}}$  is taken at the scale  $k = 0.05 \text{ Mpc}^{-1}$  (i.e.,  $k_{\text{mid}}$  in Ref [63]). We evaluate the ‘spectator-ness’ measures  $V_S/V_{\text{PBH}}$  and  $m_\chi/H$  at  $N_{\text{CMB}}$ . Observables are computed using PyTransport.

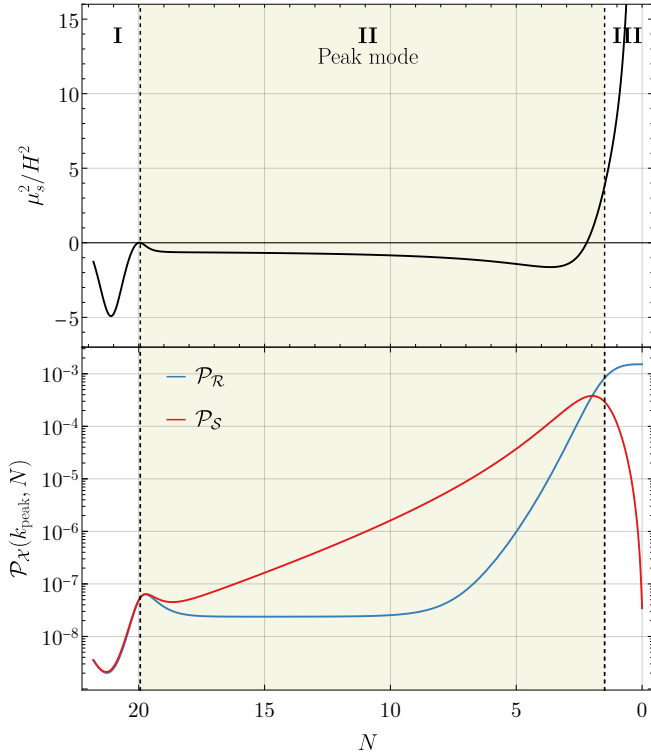


FIG. 18. Evolution of  $\mu_s^2$  and of the curvature and isocurvature perturbations  $\mathcal{R}$  and  $\mathcal{S}$ , for the  $V_{\text{PBH},B}$  potential of Eq. (50). The parameters used in the Figure are summarized in Table V.

vature power spectrum (which is broadened in PBHB), but will nevertheless be in accordance with the single-field case, since the phase of ultra-slow-roll enhancement of modes  $\mathcal{R}_k$  will also be extended. The striking similarity between the single-field and PBHspec scenarios for  $V_{\text{PBH},B}$  can be observed in Fig. 19.

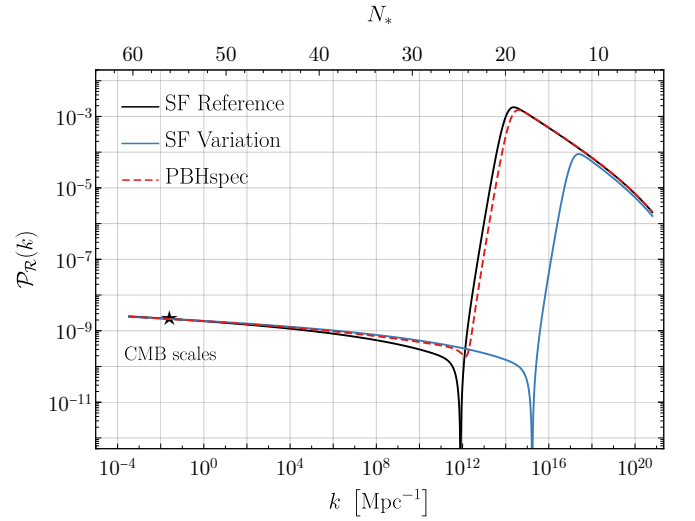


FIG. 19. Curvature power spectrum for the  $V_{\text{PBH},B}$  potential of Eq. (50). The parameters used in the Figure are summarised in Table V.

## VII. DISCUSSION

Scalar fields are ubiquitous in models of high energy physics. In the context of inflationary cosmology, scalar fields in addition to the inflaton can play the role of a *spectator field*, which does not couple to the inflaton directly and which contributes a subdominant fraction of the total energy density of the Universe. The phenomenology of inflation in the presence of spectator fields has been extensively studied (cf. [87–91]). In this work, we have extended this body of work to include spectator fields in single-field inflation models which seed primordial black holes through a phase of ultra-slow-roll (USR) evolution.

While USR models of PBH production are premised on an exponential slow-down of the inflaton and hence a sharp decrease in the slow-roll parameter  $\epsilon$ , a spectator field maintains a near-constant velocity at all times. This creates a floor for the combined total  $\epsilon$  below which the system cannot cross, and prevents the system from entering into USR. One might naively expect this to preclude the enhancement of perturbations for which these single-field models were engineered. In this work, and the companion paper [92], we have demonstrated that the enhancement survives, and moreover the spectator alleviates much of the fine-tuning of parameters required of the underlying single-field model.

The spectator qualitatively changes the dynamics of both the background and perturbations: the would-be USR phase is supplanted by a phase wherein the inflationary trajectory turns to flow along the spectator direction. Despite the spectator providing a subdominant contribution to the energy density, it briefly dominates the kinematics. This phase is characterized by tachyonic instability for isocurvature perturbations, and bracketed by turns in field space, which convert power from isocurvature perturbations to curvature perturbations, following which the isocurvature modes decay. The net result is an enhancement of the amplitude of curvature perturbations that parallels that in the single-field case.

The observables of the model are in remarkable agreement with the underlying single-field models. The power spectrum inherits the same predictions for CMB observables, the same slope of the peak of the power spectrum of PBH-relevant scales, and the same decay of the peak. As we have explained in detail in Sec. IV and VI, this commonality arises from the shared evolution of inflation fluctuations in the two models.

Where the two models differ is the extent to which the feature of the inflaton potential must be set by hand: the spectator model can accommodate a much less fine-tuned feature in the inflaton potential, by compensating  $\mathcal{O}(1)$  parameter variations of the spectator mass and initial condition. Whether this amounts to a definetuning in a

Bayesian sense requires a full statistical analysis, which is topic of future work [124].

These results are illustrated in the context of a few specific single-models—those of Refs. [39, 40, 48]—but apply broadly to any model of single-field inflation model that is minimally coupled to gravity and which realizes USR through a feature in the potential. We have demonstrated this by undertaking our analysis for second distinct and unrelated models, finding the same results: the spectator maintains or enhances the perturbations relative to the single-field models.

There are many directions for future work. Foremost among these is a detailed exploration of parameter space to quantify the fine-tuning in the spectator versus single-field models. This exploration will enable study of other parameter regimes, such as ones in which the spectator field generates a second phase of slow-roll inflation. It will also be interesting to generalize the spectator model to other spectator potentials, to multiple spectators, or to a spectator nonminimally coupled to gravity. We leave this and other interesting directions to future work.

## ACKNOWLEDGEMENTS

The authors thank Josu Aurrekoetxea, Matteo Braglia, Chris Byrnes, Bryce Cyr, Alexandra Klipfel, Jérôme Martin, Sebastien Renaux-Petel, and Vincent Vennin for helpful discussions. Portions of this research were conducted in MIT’s Center for Theoretical Physics – a Leinweber Institute and supported in part by the U.S. Department of Energy under Contract No. DE-SC0012567. E.M. is supported in part by a Discovery Grant from the Natural Sciences and Engineering Research Council of Canada, and by a New Investigator Operating Grant from Research Manitoba. S.R.G. is supported by the NSF Mathematical and Physical Sciences Ascending postdoctoral fellowship, under Award No. 2317018. D.L. is supported in part by a PhD Research Studentship from Research Manitoba.

- 
- [1] I. D. Zel’dovich, Ya.B.; Novikov, “The Hypothesis of Cores Retarded during Expansion and the Hot Cosmological Model,” *Soviet Astron. AJ (Engl. Transl. )*, **10**, 602 (1967).
  - [2] Stephen Hawking, “Gravitationally collapsed objects of very low mass,” *Mon. Not. Roy. Astron. Soc.* **152**, 75 (1971).
  - [3] Bernard J. Carr and S. W. Hawking, “Black holes in the early Universe,” *Mon. Not. Roy. Astron. Soc.* **168**, 399–415 (1974).
  - [4] P. Meszaros, “The behaviour of point masses in an expanding cosmological substratum,” *Astron. Astrophys.* **37**, 225–228 (1974).
  - [5] Bernard J. Carr, “The Primordial black hole mass spectrum,” *Astrophys. J.* **201**, 1–19 (1975).
  - [6] M. Khlopov, B. A. Malomed, and Ia. B. Zeldovich, “Gravitational instability of scalar fields and formation of primordial black holes,” *Mon. Not. Roy. Astron. Soc.* **215**, 575–589 (1985).
  - [7] Jens C. Niemeyer and K. Jedamzik, “Dynamics of primordial black hole formation,” *Phys. Rev. D* **59**, 124013 (1999), [arXiv:astro-ph/9901292](#).
  - [8] Maxim Yu. Khlopov, “Primordial Black Holes,” *Res. Astron. Astrophys.* **10**, 495–528 (2010), [arXiv:0801.0116 \[astro-ph\]](#).
  - [9] B. J. Carr, Kazunori Kohri, Yuuiti Sendouda, and Jun’ichi Yokoyama, “New cosmological constraints on primordial black holes,” *Phys. Rev. D* **81**, 104019 (2010), [arXiv:0912.5297 \[astro-ph.CO\]](#).



- [10] Misao Sasaki, Teruaki Suyama, Takahiro Tanaka, and Shuichiro Yokoyama, “Primordial black holes—perspectives in gravitational wave astronomy,” *Class. Quant. Grav.* **35**, 063001 (2018), [arXiv:1801.05235 \[astro-ph.CO\]](#).
- [11] Bernard Carr, Kazunori Kohri, Yuuiti Sendouda, and Jun’ichi Yokoyama, “Constraints on primordial black holes,” *Rept. Prog. Phys.* **84**, 116902 (2021), [arXiv:2002.12778 \[astro-ph.CO\]](#).
- [12] Bernard Carr and Florian Kühnel, “Primordial Black Holes as Dark Matter: Recent Developments,” *Ann. Rev. Nucl. Part. Sci.* **70**, 355–394 (2020), [arXiv:2006.02838 \[astro-ph.CO\]](#).
- [13] Anne M. Green and Bradley J. Kavanagh, “Primordial Black Holes as a dark matter candidate,” *J. Phys. G* **48**, 043001 (2021), [arXiv:2007.10722 \[astro-ph.CO\]](#).
- [14] Albert Escrivà, “PBH Formation from Spherically Symmetric Hydrodynamical Perturbations: A Review,” *Universe* **8**, 66 (2022), [arXiv:2111.12693 \[gr-qc\]](#).
- [15] Pablo Villanueva-Domingo, Olga Mena, and Sergio Palomares-Ruiz, “A brief review on primordial black holes as dark matter,” *Front. Astron. Space Sci.* **8**, 87 (2021), [arXiv:2103.12087 \[astro-ph.CO\]](#).
- [16] Albert Escrivà, Florian Kühnel, and Yuichiro Tada, “Primordial Black Holes,” (2022) [arXiv:2211.05767 \[astro-ph.CO\]](#).
- [17] Matthew Gorton and Anne M. Green, “How open is the asteroid-mass primordial black hole window?” *SciPost Phys.* **17**, 032 (2024), [arXiv:2403.03839 \[astro-ph.CO\]](#).
- [18] Marta Volonteri, Melanie Habouzit, and Monica Colpi, “The origins of massive black holes,” *Nature Rev. Phys.* **3**, 732–743 (2021), [arXiv:2110.10175 \[astro-ph.GA\]](#).
- [19] Pratika Dayal, “Exploring a primordial solution for early black holes detected with JWST,” *Astron. Astrophys.* **690**, A182 (2024), [arXiv:2407.07162 \[astro-ph.GA\]](#).
- [20] Huang, Hai-Long and Wang, Yu-Tong and Piao, Yun-Song, “Supermassive primordial black holes for the GHZ9 and UHZ1 observed by the JWST,” (2024), [arXiv:2410.05891 \[astro-ph.GA\]](#).
- [21] Hai-Long Huang, Jun-Qian Jiang, Jibin He, Yu-Tong Wang, and Yun-Song Piao, “Sub-Eddington accreting supermassive primordial black holes explain Little Red Dots,” (2024), [arXiv:2410.20663 \[astro-ph.GA\]](#).
- [22] Hai-Long Huang, Jun-Qian Jiang, and Yun-Song Piao, “High-redshift JWST massive galaxies and the initial clustering of supermassive primordial black holes,” *Phys. Rev. D* **110**, 103540 (2024), [arXiv:2407.15781 \[astro-ph.CO\]](#).
- [23] Simeon Bird, Ilias Cholis, Julian B. Muñoz, Yacine Ali-Haïmoud, Marc Kamionkowski, Ely D. Kovetz, Alvise Raccanelli, and Adam G. Riess, “Did LIGO detect dark matter?” *Phys. Rev. Lett.* **116**, 201301 (2016), [arXiv:1603.00464 \[astro-ph.CO\]](#).
- [24] V. De Luca, G. Franciolini, and A. Riotto, “NANOGrav Data Hints at Primordial Black Holes as Dark Matter,” *Phys. Rev. Lett.* **126**, 041303 (2021), [arXiv:2009.08268 \[astro-ph.CO\]](#).
- [25] Vitorio A. De Lorenci, David I. Kaiser, Patrick Peter, Lucas S. Ruiz, and Noah E. Wolfe, “Gravitational wave signals from primordial black holes orbiting solar-type stars,” *Phys. Rev. D* **112**, 063063 (2025), [arXiv:2504.07517 \[gr-qc\]](#).
- [26] Wenzer Qin, Sarah R. Geller, Shyam Balaji, Evan McDonough, and David I. Kaiser, “Planck constraints and gravitational wave forecasts for primordial black hole dark matter seeded by multifield inflation,” *Phys. Rev. D* **108**, 043508 (2023), [arXiv:2303.02168 \[astro-ph.CO\]](#).
- [27] Alexandra P. Klipfel and David I. Kaiser, “Ultrahigh-Energy Neutrinos from Primordial Black Holes,” *Phys. Rev. Lett.* **135**, 121003 (2025), [arXiv:2503.19227 \[hep-ph\]](#).
- [28] Michael J. Baker, Joaquim Iguaz Juan, Aidan Symons, and Andrea Thamm, “Explaining the PeV Neutrino Fluxes at KM3NeT and IceCube with Quasi-Extremal Primordial Black Holes,” (2025), [arXiv:2505.22722 \[hep-ph\]](#).
- [29] Alexandra P. Klipfel, Peter Fisher, and David I. Kaiser, “Hawking radiation signatures from primordial black holes transiting the inner Solar System: Prospects for detection,” *Phys. Rev. D* **112**, 103007 (2025), [arXiv:2506.14041 \[astro-ph.CO\]](#).
- [30] S. W. Hawking, I. G. Moss, and J. M. Stewart, “Bubble Collisions in the Very Early Universe,” *Phys. Rev. D* **26**, 2681 (1982).
- [31] Heling Deng and Alexander Vilenkin, “Primordial black hole formation by vacuum bubbles,” *JCAP* **12**, 044 (2017), [arXiv:1710.02865 \[gr-qc\]](#).
- [32] S. W. Hawking, “Black Holes From Cosmic Strings,” *Phys. Lett. B* **231**, 237–239 (1989).
- [33] Alexander Polnarev and Robert Zembowicz, “Formation of Primordial Black Holes by Cosmic Strings,” *Phys. Rev. D* **43**, 1106–1109 (1991).
- [34] Sergei G. Rubin, Alexander S. Sakharov, and Maxim Yu. Khlopov, “The Formation of primary galactic nuclei during phase transitions in the early universe,” *J. Exp. Theor. Phys.* **91**, 921–929 (2001), [arXiv:hep-ph/0106187](#).
- [35] Gia Dvali, Florian Kühnel, and Michael Zantedeschi, “Primordial black holes from confinement,” *Phys. Rev. D* **104**, 123507 (2021), [arXiv:2108.09471 \[hep-ph\]](#).
- [36] William H. Kinney, “Horizon crossing and inflation with large eta,” *Phys. Rev. D* **72**, 023515 (2005), [arXiv:gr-qc/0503017](#).
- [37] Jerome Martin, Hayato Motohashi, and Teruaki Suyama, “Ultra Slow-Roll Inflation and the non-Gaussianity Consistency Relation,” *Phys. Rev. D* **87**, 023514 (2013), [arXiv:1211.0083 \[astro-ph.CO\]](#).
- [38] Jose Maria Ezquiaga, Juan Garcia-Bellido, and Ester Ruiz Morales, “Primordial Black Hole production in Critical Higgs Inflation,” *Phys. Lett. B* **776**, 345–349 (2018), [arXiv:1705.04861 \[astro-ph.CO\]](#).
- [39] Juan Garcia-Bellido and Ester Ruiz Morales, “Primordial black holes from single field models of inflation,” *Phys. Dark Univ.* **18**, 47–54 (2017), [arXiv:1702.03901 \[astro-ph.CO\]](#).
- [40] Cristiano Germani and Tomislav Prokopec, “On primordial black holes from an inflection point,” *Phys. Dark Univ.* **18**, 6–10 (2017), [arXiv:1706.04226 \[astro-ph.CO\]](#).
- [41] Kristjan Kannike, Luca Marzola, Martti Raidal, and Hardi Veermäe, “Single Field Double Inflation and Primordial Black Holes,” *JCAP* **09**, 020 (2017), [arXiv:1705.06225 \[astro-ph.CO\]](#).
- [42] Hayato Motohashi and Wayne Hu, “Primordial Black Holes and Slow-Roll Violation,” *Phys. Rev. D* **96**, 063503 (2017), [arXiv:1706.06784 \[astro-ph.CO\]](#).

- [43] Haoran Di and Yungui Gong, “Primordial black holes and second order gravitational waves from ultra-slow-roll inflation,” *JCAP* **07**, 007 (2018), [arXiv:1707.09578 \[astro-ph.CO\]](#).
- [44] Guillermo Ballesteros and Marco Taoso, “Primordial black hole dark matter from single field inflation,” *Phys. Rev. D* **97**, 023501 (2018), [arXiv:1709.05565 \[hep-ph\]](#).
- [45] Chris Pattison, Vincent Vennin, Hooshyar Assadullahi, and David Wands, “Quantum diffusion during inflation and primordial black holes,” *JCAP* **10**, 046 (2017), [arXiv:1707.00537 \[hep-th\]](#).
- [46] Samuel Passaglia, Wayne Hu, and Hayato Motohashi, “Primordial black holes and local non-Gaussianity in canonical inflation,” *Phys. Rev. D* **99**, 043536 (2019), [arXiv:1812.08243 \[astro-ph.CO\]](#).
- [47] Matteo Biagetti, Gabriele Franciolini, Alex Kehagias, and Antonio Riotto, “Primordial Black Holes from Inflation and Quantum Diffusion,” *JCAP* **07**, 032 (2018), [arXiv:1804.07124 \[astro-ph.CO\]](#).
- [48] Swagat S. Mishra and Varun Sahni, “Primordial Black Holes from a tiny bump/dip in the Inflaton potential,” *JCAP* **04**, 007 (2020), [arXiv:1911.00057 \[gr-qc\]](#).
- [49] Daniel G. Figueroa, Sami Raatikainen, Syksy Rasanen, and Eemeli Tomberg, “Non-Gaussian Tail of the Curvature Perturbation in Stochastic Ultraslow-Roll Inflation: Implications for Primordial Black Hole Production,” *Phys. Rev. Lett.* **127**, 101302 (2021), [arXiv:2012.06551 \[astro-ph.CO\]](#).
- [50] Alexandros Karam, Niko Koivunen, Eemeli Tomberg, Ville Vaskonen, and Hardi Veermäe, “Anatomy of single-field inflationary models for primordial black holes,” *JCAP* **03**, 013 (2023), [arXiv:2205.13540 \[astro-ph.CO\]](#).
- [51] Ogan Özsoy and Gianmassimo Tasinato, “Inflation and Primordial Black Holes,” *Universe* **9**, 203 (2023), [arXiv:2301.03600 \[astro-ph.CO\]](#).
- [52] Philippa S. Cole, Andrew D. Gow, Christian T. Byrnes, and Subodh P. Patil, “Primordial black holes from single-field inflation: a fine-tuning audit,” *JCAP* **08**, 031 (2023), [arXiv:2304.01997 \[astro-ph.CO\]](#).
- [53] Michele Cicoli, Victor A. Diaz, and Francisco G. Pedro, “Primordial Black Holes from String Inflation,” *JCAP* **06**, 034 (2018), [arXiv:1803.02837 \[hep-th\]](#).
- [54] Michele Cicoli, Francisco G. Pedro, and Nicola Pedron, “Secondary GWs and PBHs in string inflation: formation and detectability,” *JCAP* **08**, 030 (2022), [arXiv:2203.00021 \[hep-th\]](#).
- [55] Yi-Fu Cai, Xiao-Han Ma, Misao Sasaki, Dong-Gang Wang, and Zihan Zhou, “Highly non-Gaussian tails and primordial black holes from single-field inflation,” *JCAP* **12**, 034 (2022), [arXiv:2207.11910 \[astro-ph.CO\]](#).
- [56] Keisuke Inomata, Evan McDonough, and Wayne Hu, “Primordial black holes arise when the inflaton falls,” *Phys. Rev. D* **104**, 123553 (2021), [arXiv:2104.03972 \[astro-ph.CO\]](#).
- [57] Keisuke Inomata, Evan McDonough, and Wayne Hu, “Amplification of primordial perturbations from the rise or fall of the inflaton,” *JCAP* **02**, 031 (2022), [arXiv:2110.14641 \[astro-ph.CO\]](#).
- [58] Nilanjandev Bhaumik and Rajeev Kumar Jain, “Primordial black holes dark matter from inflection point models of inflation and the effects of reheating,” *JCAP* **01**, 037 (2020), [arXiv:1907.04125 \[astro-ph.CO\]](#).
- [59] Shi Pi and Misao Sasaki, “Logarithmic Duality of the Curvature Perturbation,” *Phys. Rev. Lett.* **131**, 011002 (2023), [arXiv:2211.13932 \[astro-ph.CO\]](#).
- [60] Sayantan Choudhury, Ahaskar Karde, Sudhakar Panda, and M. Sami, “Realisation of the ultra-slow roll phase in Galileon inflation and PBH overproduction,” *JCAP* **07**, 034 (2024), [arXiv:2401.10925 \[astro-ph.CO\]](#).
- [61] Y. Akrami *et al.* (Planck), “Planck 2018 results. IX. Constraints on primordial non-Gaussianity,” *Astron. Astrophys.* **641**, A9 (2020), [arXiv:1905.05697 \[astro-ph.CO\]](#).
- [62] N. Aghanim *et al.* (Planck), “Planck 2018 results. VI. Cosmological parameters,” *Astron. Astrophys.* **641**, A6 (2020), [Erratum: *Astron. Astrophys.* 652, C4 (2021)], [arXiv:1807.06209 \[astro-ph.CO\]](#).
- [63] Y. Akrami *et al.* (Planck), “Planck 2018 results. X. Constraints on inflation,” *Astron. Astrophys.* **641**, A10 (2020), [arXiv:1807.06211 \[astro-ph.CO\]](#).
- [64] P. A. R. Ade *et al.* (BICEP, Keck), “Improved Constraints on Primordial Gravitational Waves using Planck, WMAP, and BICEP/Keck Observations through the 2018 Observing Season,” *Phys. Rev. Lett.* **127**, 151301 (2021), [arXiv:2110.00483 \[astro-ph.CO\]](#).
- [65] G. C. Branco, P. M. Ferreira, L. Lavoura, M. N. Rebelo, Marc Sher, and Joao P. Silva, “Theory and phenomenology of two-Higgs-doublet models,” *Phys. Rept.* **516**, 1–102 (2012), [arXiv:1106.0034 \[hep-ph\]](#).
- [66] David H. Lyth and Antonio Riotto, “Particle physics models of inflation and the cosmological density perturbation,” *Phys. Rept.* **314**, 1–146 (1999), [arXiv:hep-ph/9807278](#).
- [67] Anupam Mazumdar and Jonathan Rocher, “Particle physics models of inflation and curvaton scenarios,” *Phys. Rept.* **497**, 85–215 (2011), [arXiv:1001.0993 \[hep-ph\]](#).
- [68] Sebastian Vander Ploeg Fallon, James Halverson, Liam McAllister, and Yunhao Zhu, “F-theory Axiverse,” (2025), [arXiv:2511.20458 \[hep-th\]](#).
- [69] Evan McDonough, Alan H. Guth, and David I. Kaiser, “Nonminimal Couplings and the Forgotten Field of Axion Inflation,” (2020), [arXiv:2010.04179 \[hep-th\]](#).
- [70] Azadeh Maleknejad and Evan McDonough, “Ultralight pion and superheavy baryon dark matter,” *Phys. Rev. D* **106**, 095011 (2022), [arXiv:2205.12983 \[hep-ph\]](#).
- [71] Stephon Alexander, Humberto Gilmer, Tucker Manton, and Evan McDonough, “ $\pi$ -axion and  $\pi$ -axiverse of dark QCD,” *Phys. Rev. D* **108**, 123014 (2023), [arXiv:2304.11176 \[hep-ph\]](#).
- [72] Stephon Alexander, Tucker Manton, and Evan McDonough, “Field theory axiverse,” *Phys. Rev. D* **109**, 116019 (2024), [arXiv:2404.11642 \[hep-ph\]](#).
- [73] Lisa Randall, Marin Soljatic, and Alan H. Guth, “Supernatural inflation: Inflation from supersymmetry with no (very) small parameters,” *Nucl. Phys. B* **472**, 377–408 (1996), [arXiv:hep-ph/9512439](#).
- [74] Juan Garcia-Bellido, Andrei D. Linde, and David Wands, “Density perturbations and black hole formation in hybrid inflation,” *Phys. Rev. D* **54**, 6040–6058 (1996), [arXiv:astro-ph/9605094](#).
- [75] David H. Lyth, “Contribution of the hybrid inflation waterfall to the primordial curvature perturbation,” *JCAP* **07**, 035 (2011), [arXiv:1012.4617 \[astro-ph.CO\]](#).
- [76] Edgar Bugaev and Peter Klimai, “Formation of primordial black holes from non-Gaussian perturbations

- produced in a waterfall transition,” *Phys. Rev. D* **85**, 103504 (2012), [arXiv:1112.5601 \[astro-ph.CO\]](#).
- [77] Illan F. Halpern, Mark P. Hertzberg, Matthew A. Joss, and Evangelos I. Sfakianakis, “A Density Spike on Astrophysical Scales from an N-Field Waterfall Transition,” *Phys. Lett. B* **748**, 132–143 (2015), [arXiv:1410.1878 \[astro-ph.CO\]](#).
- [78] Sébastien Clesse and Juan García-Bellido, “Massive Primordial Black Holes from Hybrid Inflation as Dark Matter and the seeds of Galaxies,” *Phys. Rev. D* **92**, 023524 (2015), [arXiv:1501.07565 \[astro-ph.CO\]](#).
- [79] Masahiro Kawasaki and Yuichiro Tada, “Can massive primordial black holes be produced in mild waterfall hybrid inflation?” *JCAP* **08**, 041 (2016), [arXiv:1512.03515 \[astro-ph.CO\]](#).
- [80] Matteo Braglia, Andrei Linde, Renata Kallosh, and Fabio Finelli, “Hybrid  $\alpha$ -attractors, primordial black holes and gravitational wave backgrounds,” *JCAP* **04**, 033 (2023), [arXiv:2211.14262 \[astro-ph.CO\]](#).
- [81] Jacopo Fumagalli, Sébastien Renaux-Petel, John W. Ronayne, and Lukas T. Witkowski, “Turning in the landscape: A new mechanism for generating primordial black holes,” *Phys. Lett. B* **841**, 137921 (2023), [arXiv:2004.08369 \[hep-th\]](#).
- [82] Matteo Braglia, Dhiraj Kumar Hazra, Fabio Finelli, George F. Smoot, L. Sriramkumar, and Alexei A. Starobinsky, “Generating PBHs and small-scale GWs in two-field models of inflation,” *JCAP* **08**, 001 (2020), [arXiv:2005.02895 \[astro-ph.CO\]](#).
- [83] Gonzalo A. Palma, Spyros Sypsas, and Cristobal Zenteno, “Seeding primordial black holes in multi-field inflation,” *Phys. Rev. Lett.* **125**, 121301 (2020), [arXiv:2004.06106 \[astro-ph.CO\]](#).
- [84] Sarah R. Geller, Wenzer Qin, Evan McDonough, and David I. Kaiser, “Primordial black holes from multi-field inflation with nonminimal couplings,” *Phys. Rev. D* **106**, 063535 (2022), [arXiv:2205.04471 \[hep-th\]](#).
- [85] Paulo B. Ferraz and João G. Rosa, “The inflation trilogy and primordial black holes,” *JCAP* **03**, 040 (2025), [arXiv:2410.10996 \[hep-ph\]](#).
- [86] Sukannya Bhattacharya and Ivonne Zavala, “Sharp turns in axion monodromy: primordial black holes and gravitational waves,” *JCAP* **04**, 065 (2023), [arXiv:2205.06065 \[astro-ph.CO\]](#).
- [87] Xingang Chen, Gonzalo A. Palma, Walter Riquelme, Bruno Scheihing Hitschfeld, and Spyros Sypsas, “Landscape tomography through primordial non-Gaussianity,” *Phys. Rev. D* **98**, 083528 (2018), [arXiv:1804.07315 \[hep-th\]](#).
- [88] Emanuela Dimastrogiovanni, Matteo Fasiello, and Tomohiro Fujita, “Primordial Gravitational Waves from Axion-Gauge Fields Dynamics,” *JCAP* **01**, 019 (2017), [arXiv:1608.04216 \[astro-ph.CO\]](#).
- [89] Evan McDonough and Stephon Alexander, “Observable Chiral Gravitational Waves from Inflation in String Theory,” *JCAP* **11**, 030 (2018), [arXiv:1806.05684 \[hep-th\]](#).
- [90] Jonathan Holland, Ivonne Zavala, and Gianmassimo Tasinato, “On chromonatural inflation in string theory,” *JCAP* **12**, 026 (2020), [arXiv:2009.00653 \[hep-th\]](#).
- [91] Stephon Alexander, Evan McDonough, and David N. Spergel, “Chiral Gravitational Waves and Baryon Superfluid Dark Matter,” *JCAP* **05**, 003 (2018), [arXiv:1801.07255 \[hep-th\]](#).
- [92] Dario L. Lorenzoni, Sarah R. Geller, Zachary Ireland, David I. Kaiser, Evan McDonough, and Kyle A. Wittmeier, “Light Scalar Fields Foster Production of Primordial Black Holes,” (2025), [arXiv:2504.13251 \[astro-ph.CO\]](#).
- [93] Shamit Kachru, Renata Kallosh, Andrei D. Linde, and Sandip P. Trivedi, “De Sitter vacua in string theory,” *Phys. Rev. D* **68**, 046005 (2003), [arXiv:hep-th/0301240](#).
- [94] Misao Sasaki and Ewan D. Stewart, “A General analytic formula for the spectral index of the density perturbations produced during inflation,” *Prog. Theor. Phys.* **95**, 71–78 (1996), [arXiv:astro-ph/9507001](#).
- [95] Christopher Gordon, David Wands, Bruce A. Bassett, and Roy Maartens, “Adiabatic and entropy perturbations from inflation,” *Phys. Rev. D* **63**, 023506 (2000), [arXiv:astro-ph/0009131](#).
- [96] David Wands, Nicola Bartolo, Sabino Matarrese, and Antonio Riotto, “An Observational test of two-field inflation,” *Phys. Rev. D* **66**, 043520 (2002), [arXiv:astro-ph/0205253](#).
- [97] David Langlois and Sébastien Renaux-Petel, “Perturbations in generalized multi-field inflation,” *JCAP* **04**, 017 (2008), [arXiv:0801.1085 \[hep-th\]](#).
- [98] Courtney M. Peterson and Max Tegmark, “Testing Two-Field Inflation,” *Phys. Rev. D* **83**, 023522 (2011), [arXiv:1005.4056 \[astro-ph.CO\]](#).
- [99] Jinn-Ouk Gong and Takahiro Tanaka, “A covariant approach to general field space metric in multi-field inflation,” *JCAP* **03**, 015 (2011), [Erratum: *JCAP* **02**, E01 (2012)], [arXiv:1101.4809 \[astro-ph.CO\]](#).
- [100] David I. Kaiser, Edward A. Mazenc, and Evangelos I. Sfakianakis, “Primordial Bispectrum from Multifield Inflation with Nonminimal Couplings,” *Phys. Rev. D* **87**, 064004 (2013), [arXiv:1210.7487 \[astro-ph.CO\]](#).
- [101] Jinn-Ouk Gong, “Multi-field inflation and cosmological perturbations,” *Int. J. Mod. Phys. D* **26**, 1740003 (2016), [arXiv:1606.06971 \[gr-qc\]](#).
- [102] David I. Kaiser and Evangelos I. Sfakianakis, “Multifield Inflation after Planck: The Case for Nonminimal Couplings,” *Phys. Rev. Lett.* **112**, 011302 (2014), [arXiv:1304.0363 \[astro-ph.CO\]](#).
- [103] Katelin Schutz, Evangelos I. Sfakianakis, and David I. Kaiser, “Multifield Inflation after Planck: Isocurvature Modes from Nonminimal Couplings,” *Phys. Rev. D* **89**, 064044 (2014), [arXiv:1310.8285 \[astro-ph.CO\]](#).
- [104] Mafalda Dias, Jonathan Frazer, David J. Mulryne, and David Seery, “Numerical evaluation of the bispectrum in multiple field inflation—the transport approach with code,” *JCAP* **12**, 033 (2016), [arXiv:1609.00379 \[astro-ph.CO\]](#).
- [105] David J. Mulryne and John W. Ronayne, “PyTransport: A Python package for the calculation of inflationary correlation functions,” *J. Open Source Softw.* **3**, 494 (2018), [arXiv:1609.00381 \[astro-ph.CO\]](#).
- [106] Mafalda Dias, Jonathan Frazer, and David Seery, “Computing observables in curved multifield models of inflation—A guide (with code) to the transport method,” *JCAP* **12**, 030 (2015), [arXiv:1502.03125 \[astro-ph.CO\]](#).
- [107] Ana Achúcarro, Jinn-Ouk Gong, Sjoerd Hardeman, Gonzalo A. Palma, and Subodh P. Patil, “Features of heavy physics in the CMB power spectrum,” *JCAP* **01**, 030 (2011), [arXiv:1010.3693 \[hep-ph\]](#).

- [108] Christian T. Byrnes, Philippa S. Cole, and Subodh P. Patil, “Steepest growth of the power spectrum and primordial black holes,” *JCAP* **06**, 028 (2019), [arXiv:1811.11158 \[astro-ph.CO\]](#).
- [109] Sam Young, Ilia Musco, and Christian T. Byrnes, “Primordial black hole formation and abundance: contribution from the non-linear relation between the density and curvature perturbation,” *JCAP* **11**, 012 (2019), [arXiv:1904.00984 \[astro-ph.CO\]](#).
- [110] Alex Kehagias, Ilia Musco, and Antonio Riotto, “Non-Gaussian Formation of Primordial Black Holes: Effects on the Threshold,” *JCAP* **12**, 029 (2019), [arXiv:1906.07135 \[astro-ph.CO\]](#).
- [111] Albert Escrivà, Cristiano Germani, and Ravi K. Sheth, “Universal threshold for primordial black hole formation,” *Phys. Rev. D* **101**, 044022 (2020), [arXiv:1907.13311 \[gr-qc\]](#).
- [112] V. De Luca, G. Franciolini, and A. Riotto, “On the Primordial Black Hole Mass Function for Broad Spectra,” *Phys. Lett. B* **807**, 135550 (2020), [arXiv:2001.04371 \[astro-ph.CO\]](#).
- [113] Ilia Musco, Valerio De Luca, Gabriele Franciolini, and Antonio Riotto, “Threshold for primordial black holes. II. A simple analytic prescription,” *Phys. Rev. D* **103**, 063538 (2021), [arXiv:2011.03014 \[astro-ph.CO\]](#).
- [114] Scott Dodelson and Lam Hui, “A Horizon ratio bound for inflationary fluctuations,” *Phys. Rev. Lett.* **91**, 131301 (2003), [arXiv:astro-ph/0305113](#).
- [115] Andrew R Liddle and Samuel M Leach, “How long before the end of inflation were observable perturbations produced?” *Phys. Rev. D* **68**, 103503 (2003), [arXiv:astro-ph/0305263](#).
- [116] Mustafa A. Amin, Mark P. Hertzberg, David I. Kaiser, and Johanna Karouby, “Nonperturbative Dynamics Of Reheating After Inflation: A Review,” *Int. J. Mod. Phys. D* **24**, 1530003 (2014), [arXiv:1410.3808 \[hep-ph\]](#).
- [117] Jessica L. Cook, Emanuela Dimastrogiovanni, Damien A. Easson, and Lawrence M. Krauss, “Reheating predictions in single field inflation,” *JCAP* **04**, 047 (2015), [arXiv:1502.04673 \[astro-ph.CO\]](#).
- [118] Jerome Martin, Christophe Ringeval, and Vincent Vennin, “Information Gain on Reheating: the One Bit Milestone,” *Phys. Rev. D* **93**, 103532 (2016), [arXiv:1603.02606 \[astro-ph.CO\]](#).
- [119] Rouzbeh Allahverdi *et al.*, “The First Three Seconds: a Review of Possible Expansion Histories of the Early Universe,” *Open J. Astrophys.* **4** (2020), 10.21105/astro.2006.16182, [arXiv:2006.16182 \[astro-ph.CO\]](#).
- [120] P. A. R. Ade *et al.* (Planck), “Planck 2015 results. XX. Constraints on inflation,” *Astron. Astrophys.* **594**, A20 (2016), [arXiv:1502.02114 \[astro-ph.CO\]](#).
- [121] Eiichiro Komatsu and David N. Spergel, “Acoustic signatures in the primary microwave background bispectrum,” *Phys. Rev. D* **63**, 063002 (2001), [arXiv:astro-ph/0005036](#).
- [122] J. R. Fergusson and Edward P. S. Shellard, “Primordial non-Gaussianity and the CMB bispectrum,” *Phys. Rev. D* **76**, 083523 (2007), [arXiv:astro-ph/0612713](#).
- [123] G. I. Rigopoulos, E. P. S. Shellard, and B. J. W. van Tent, “A Simple route to non-Gaussianity in inflation,” *Phys. Rev. D* **72**, 083507 (2005), [arXiv:astro-ph/0410486](#).
- [124] Param Upadhyaya, Dario L. Lorenzoni, Sarah R. Geller, David I. Kaiser, and Evan McDonough, In prep.
- [125] Fedor L. Bezrukov and Mikhail Shaposhnikov, “The Standard Model Higgs boson as the inflaton,” *Phys. Lett. B* **659**, 703–706 (2008), [arXiv:0710.3755 \[hep-th\]](#).